The Thesis committee for Evan Michael Ogden

certifies that this is the approved version of the following thesis:

A Kinematic Model of the Shoulder Complex for Estimating Shoulder Girdle Angles without Acromial Sensing

APPROVED BY

SUPERVISING COMMITTEE:

Supervisor: Ashish D. Deshpande

James Sulzer

A Kinematic Model of the Shoulder Complex for Estimating Shoulder Girdle Angles without Acromial Sensing

by

Evan Michael Ogden

THESIS

Presented to the Faculty of the Graduate School of

The University of Texas at Austin

in Partial Fulfillment

of the Requirements

for the Degree of

Master of Science in Engineering

THE UNIVERSITY OF TEXAS AT AUSTIN

August 2017

To my brother, Bradley. As you prepare for a future career in physical therapy, I remind myself that my work should make your job better, not take it away.

Acknowledgments

First, I thank Ashish Deshpande for serving as my graduate advisor. His advice and support have been instrumental to my graduate studies and research.

I thank the present and former members of the ReNeu Robotics Lab for their help with both this work and my other research efforts. I thank the other members of the Harmony team their support and review of this theses. I thank the Cockrell School of Engineering and the Cockrell Foundation for their financial support through the Virginia & Ernest Cockrell, Jr. Fellowship in Engineering.

I also thank the National Aeronautics and Space Administration for supporting the past year of my graduate studies through a Space Technology Research Fellowship. I thank Sudhakar Rajulu, the Anthropometry and Biomechanics Facility, and other members of NASA Johnson Space Center for the technical advice and welcoming atmosphere during my visit this past May and June.

Finally, I thank my family for their love, support, and encouragement.

A Kinematic Model of the Shoulder Complex for Estimating Shoulder Girdle Angles without Acromial Sensing

by

Evan Michael Ogden, M.S.E.
The University of Texas at Austin, 2017

Supervisor: Ashish D. Deshpande

The movements of each joint in the shoulder complex is important to measure for studying shoulder function, injuries, and rehabilitation. The current standards for measuring these motions are non-invasive motion capture of surface markers or regression equations from other research studies. Certain environments, such as robotic exoskeletons and spacesuits, are not compatible with motion capture systems because their hardware obscures or precludes these measurement. The existing regression models are generalized across a wide range of subjects and are designed with experimental data that has minimal environmental interaction. So, these methods are insufficient for estimating shoulder girdle motion in an occluded setting and with substantial human-device interaction. The objective of this thesis is to develop and evaluate a novel kinematic shoulder model that estimates shoulder girdle angles without acromial sensors. This model leverages the geometric similarities of the human shoulder and a RRSS spatial linkage to constrain the internal degrees of freedom of the shoulder mechanism. A nonlinear optimization method is used to predict the configuration of the shoulder by matching desired distances between the scapula and the

ribcage. This model is validated using experimental measurements of 77 arm movements from five subjects. With ideal inputs, the kinematic model is able to accurately estimate shoulder girdle angles within 2°. The model was also able to outperform two existing shoulder regression models. However, small changes to model geometry or input kinematics result in significant errors in all shoulder angles. This is likely due to the rigidity of the kinematic constraint, which uses an idealized mechanical model to represent a complex biological system with flexible joints. Ultimately, this work shows that the kinematic constraints from this linkage model can be used to predict shoulder angles during a variety of different movements without sensors on the acromion. The model's robustness can be improved by pairing it with a compliant joint model to permit errors in anthropometry and input kinematics.

Table of Contents

List of Tables

List of Figures

Chapter 1

Introduction

The shoulder is one of the most complicated joint arrangements in the human body. This set of joints is required to display a combination of high mobility and substantial force generation. These goals are accomplished by combining highly mobile joints, a multiarticular muscle arrangement, and neuromuscular coordination patterns. Shoulder injury and rehabilitation remains an area of continued research interest, and several routes for future exploration have been identified [56, 81].

A key part of this research measuring the kinematics of the shoulder complex, including the shoulder girdle. In the clinical environment, shoulder girdle movement is critical to understanding shoulder function, recognizing past or potential injuries, and assessing therapy outcomes. Measuring shoulder motion has recently become an area of interest to both rehabilitation exoskeletons and spacesuit evaluation. Rehabilitation robots use patient kinematics to control actuation commands and measure functional progress. Erroneous measurement of this motion carries an increased risk of harmful interaction with patients or incorrect measurement of recovery. Similarly, spacesuit testing relies on crewmember kinematic data to anticipate functional performance on upcoming missions. Inaccurate assessment of shoulder motion can lead to poor fitting of suit components and higher incidence shoulder impingement.

Although both these areas require accurate shoulder kinematics, they are unable to use existing measurement methods from shoulder biomechanics research. Vi-

sual occlusion, small clearance volumes, and material interference of the exoskeletons and spacesuits limit the use of standard non-invasive methods. Invasive methods are difficult to implement alongside spacesuit or robot hardware and cannot be justified in these populations due to the long-term health risks. So, both of these fields are restricted to coarse estimates of the shoulder girdle configuration. These estimates use regression models that are developed from other populations and environments, accepting the limited generalizability of these models across conditions. Existing kinematic models have been developed to solve different problems, such as reachable workspace or segment length estimation, and require shoulder girdle angles as inputs. This is one of the key barriers to improving the safety and compatibility of these devices. A numerical model that can estimate the configuration of the shoulder in presence of occlusion and other sensor restrictions around the shoulder girdle would increase the available information about shoulder movements and device interaction.

1.1 Shoulder Physiology and Biomechanics

Before developing a model of the shoulder girdle, its structure and actuation must be understood. The appendicular shoulder skeleton includes the clavicle, scapula, and humerus. These three bones are connected in a serial chain to the axial skeleton by three synovial joints: the sternoclavicular (SC), acromioclavicular (AC), and glenohumeral (GH) joints. These joints display three rotations, similar to mechanical spherical joints, and most biomechanics research treats the rotation axes as intersecting a common point [122]. Each of the synovial articulations has both joint capsules and extracapsular ligaments for stabilizing movements. These ligaments are considered the primary stabilizers of the SC and AC joints [16]. However, the GH joint ligaments and other articular structures, such as the glenoid labrum, are considered

insufficient for providing stability to humeral head [95]. Instead, the proprioceptive contributions of the GH ligaments support active stabilization of the joint by the shoulder muscles [53, 89].

The majority of shoulder muscles attach to either the scapula or humerus. The two axiohumeral muscles, pectoralis major and latissimus dorsi, contribute towards adduction and transverse movements of the arm. So, motions involving arm elevation must involve the numerous scapulohumeral muscles. Four of these, the supraspinatus, infraspinatus, subscapularis, and teres minor, form the rotator cuff muscle group. They provide dynamic stability to the GH joint and control axial rotation of the humerus. The remaining scapulohumeral muscles, such as the biceps brachii and deltoid, contribute to humeral elevation and other arm movements.

The axioscapular muscles, along with the clavicle, transfer loads on the scapula to the axial skeleton. This completes the force transfer between the humerus and torso and allow for stable arm motion in a variety of tasks. Since there are no axioscapular ligaments, these muscles are also responsible for pulling the scapula against the thorax. This interaction between the ribs and scapula, while not a typical skeletal articulation, is called the scapulothoracic (ST) joint. Both passive and active force generation in the axioscapular muscles, particularly the rhomboids and serratus anterior, bring the medial border of the scapula towards the ribcage [88].

These muscles are also responsible for controlling the motion of the scapula. Although it is possible to train subjects to contract portions of these muscles individually, this type of muscle activity is an emerging area of research and requires biofeedback training [47, 48]. Instead, the axioscapular muscles are typically utilized to perform independent shoulder girdle motions, such as shrugging, or change the

configuration of the scapula during arm movement. Researchers have observed a consistent movement relationship between the elevation of the humerus and the motion of the scapula. As the humerus elevates, the scapula translates and rotates upward, resulting in translation of the GH joint. This coordination has been termed scapulohumeral rhythm (SHR) [15, 52]. This coordination is hypothesized to serve multiple biomechanical functions. SHR allows for a more stable GH joint while maintaining overall shoulder mobility by rotating the glenoid to a more supportive position [77]. This coordination also ensures proper muscle lengths are maintained for adequate force generation [52]. It has been recently postulated that SHR also allows for dynamic robustness when dealing with varying loads and perturbations [81].

The coordination ratios described by SHR have been found to depend on a variety of factors. Besides the variations among subjects [4], the movement pattern depends on the motion being performed. For example, humeral abduction motions have greater upward rotation of the scapula than in flexion or scapular plane elevation [70]. SHR also depends on the direction of motion being measured, as different scapular angles have been measured between raising and lowering the arm. This may be due to gravitational loading affecting the eccentric contraction of the shoulder musculature [79]. Similarly, SHR during humeral elevation is affected by the amount of external force applied to the arm [19,83]. The velocity of movement also contributes to SHR variation, although the significance of this contribution is debated [20, 34]. Muscular fatigue also affects this coordination, leading to increased ST motion in a seemingly compensatory manner [27, 35, 82].

This coordination is disrupted in patients with shoulder injuries. One of the most commonly studied conditions that presents this behavior is subacromial impinge-

ment syndrome [86]. Patients with both this and other joint injuries show altered scapular kinematics during humeral elevation [64, 77], which may lead to impaired function and GH stability. However, one of the unresolved questions with studying these impairments is determining the differences in correlation and causation between altered coordination and shoulder pain [55,56]. It is uncertain whether this dyskinesia causes shoulder pain, is a compensatory response to the pain, or is caused by some other factor.

This motion is also disrupted in patients with neuromuscular injuries, such as stroke. Stroke patients show substantially altered shoulder kinematics and reduced active range of motion on the paretic side, potentially leading to adoption of compensatory movement strategies [103, 105]. This impaired neuromuscular control is often associated with secondary musculoskeletal shoulder injuries, such as GH subluxation and shoulder pain [41,93]. However, these ancillary injuries share the similar causality questions as normal musculoskeletal injuries. Measuring the shoulder motion of these patients is important for designing treatments methods that maximize recovery.

1.2 Robotic Rehabilitation for the Upper Limb

There has been increasing interest in using robotic devices for rehabilitation after neuromuscular insults. For example, they are being considered for providing motion therapy for patient populations such as stroke, spinal cord injury, and cerebral palsy [72]. These robots have the potential to offload some of the physical burdens on the therapist, supplement current assessment methods with sensor measurements, and perform a variety of new and existing tasks with high repeatability. At least twenty randomized clinical trials have been performed with these robots for improving

arm function, and they are currently capable of increasing the speed of recovery and providing statistically significant gains in certain metrics [59, 84].

In the past two decades, the field has advanced from the earliest designs and experiments to a plethora of complex devices and dozens of clinical trials. Recent research in this area has focused on increasing robot capabilities through new joint arrangements and more complex control strategies [68]. A survey by Maciejasz et al. found that over 60 devices have been developed assisting in shoulder motion [73]. The vast majority of these devices are either end-effector systems or exoskeleton systems. End effector systems are generally simpler to design, produce, and adjust for patients. But, they have limited ability to control individual angles of the kinematically redundant upper limb, particularly shoulder girdle angles. In contrast, exoskeletons are capable of more direct control on user joint angles and torques at the cost of increased volume and complexity. Their structure and actuation allows for targeted single joint exercises motions and improved support for coordinated movements involving multiple joints [68].

Most of the exoskeletons with shoulder motion reduce the shoulder complex to the GH joint, which neglects shoulder girdle motions such as SHR. This either constrains the exoskeleton to be used in small workspaces, limiting the types of exercises available and potential therapeutic benefit, or increases the risk of impingement when the arm is elevated without proper movement of the scapula [86]. A handful of devices are capable of actively driving motion of the shoulder girdle, but they are limited to mechanically programmed shoulder coordination patterns or do not describe any specific methods for supporting coordinated shoulder motion [17, 90, 100, 115]. Although the impact of shoulder girdle motion on traditional therapy outcomes is still being

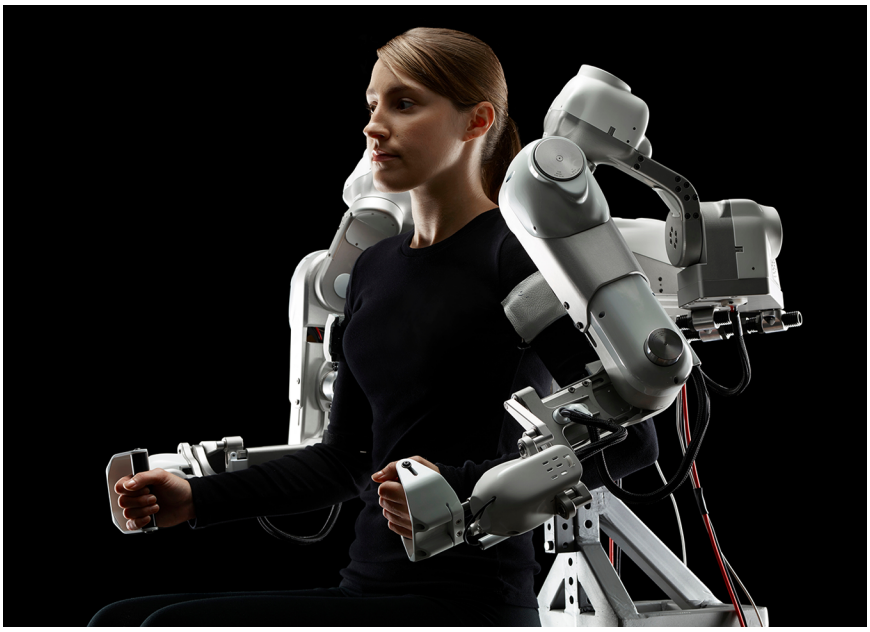

Figure 1.1: The Harmony rehabilitation exoskeleton.

studied [56, 81, 94], its importance to improving the efficacy of rehabilitation robots is unknown due to limited device capabilities.

In the Rehabilitation and Neuromuscular Robotics Lab, we have developed an upper body exoskeleton called Harmony [58] (Figure 1.1). This robot is a bilateral device with seven active degrees of freedom (DOF) per side, including five DOF for the shoulder complex. These DOF contain rotary series elastic actuators, allowing for improved torque control and safe application of forces on the shoulder. This exoskeleton is capable of actively controlling both the rotation and translation of the humeral head with two active DOF for the shoulder girdle. These proximal joints are designed to support and correct shoulder coordination during functional tasks. The robot utilizes a software control strategy for encouraging this coordination in a compliant manner [57].

Although Harmony has advanced mechanical design and actuation properties, its measurement of shoulder motion is limited in comparison to traditional biomechanics studies. The extant control strategy uses the position of the humeral head as an analogue for scapular orientation. This obscures the actual behavior of the scapula, as distinguishing between shoulder girdle elevation and scapular upward rotation is not possible[1]. These movements are important to recognize in therapy to determine if recovery or compensation is occurring, and stroke patients shown compensatory patterns at the torso [105]. Measurement of shoulder girdle angles would reveal the relative contributions of independent and coordinated shoulder motion, which would allow for exoskeleton controllers to properly adjust the movements of the patient.

1.3 NASA Spacesuits and the Shoulder

Safe and effective use of the upper limbs inside spacesuits has been a continuing challenge and is impaired by suit pressurization, fitting issues, and fatigue [119]. Measuring suited crewmember performance is a critical part of evaluating the fit quality between a crewmember and the spacesuit. This allows for missions to be completed safely and readily when encountering the numerous challenges associated with working in a pressurized suit for long durations [38]. These evaluations include assessments of range of motion, joint torques, suit fit, metabolics, and task performance [104].

While these evaluations are intended to improve suit compatibility and safety, shoulder injuries have become increasingly common among astronauts in recent years. These injuries are associated with both training for and performing spacewalks, also

[1]Part of this uncertainty is due to the 2-DOF simplification of humeral head motion. The impact of this can be studied in future research.

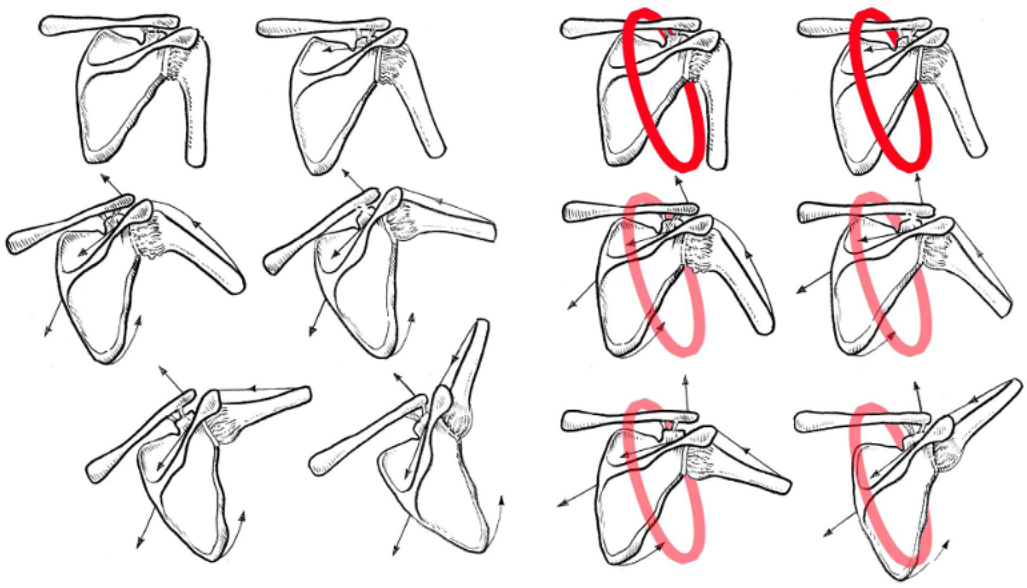

Figure 1.2: Restriction on shoulder girdle motion by the HUT shoulder bearing. Reprinted from [119].

known as extravehicular activities (EVA). Previous studies have shown that astronauts that are trained for EVA have significant incidence rates for shoulder injury and surgical intervention while using the current spacesuit design, the Extravehicular Mobility Unit (EMU) [107,119]. This research proposed that the design of certain suit components of the EMU, namely the Hard Upper Torso (HUT), were contributing factors for astronauts developing shoulder issues. The shoulder bearing of the HUT limits the amount of vertical shoulder translation, which is shown qualitatively in Figure 1.2 and increases the risk of subacromial impingement. An alternate version of the HUT is available to use during training, but this design cannot be used during spaceflight due to an increased risk of life-threatening suit failure [119]. In order to better prepare for actual EVA missions, astronauts only switch to this second design once shoulder injury or pain occurs [107].

NASA has devoted resources towards understanding how the EMU affects astronaut shoulder health in existing and upcoming designs [1, 3, 6, 42]. One of the primary impediments to resolving this is the difficulty of measuring upper limb motion while inside the EMU. Occlusion restricts the use of optical motion capture to suit-level assessment of mobility and task performance. Previous research details an in-suit system for measuring interaction forces between the upper limb and the suit as well as upper limb kinematics within the suit [2, 6]. While humeral kinematics are a recent addition to suited performance assessment, the shoulder girdle angles remain unmeasured. A model that estimates the shoulder configuration from humeral kinematics testing can lead to improved suit evaluation methods and reduced risk of crewmember injury.

1.4 Shoulder Angle Measurement Methods

Both robotic exoskeletons and spacesuits stand to benefit from measuring shoulder girdle angles. However, measuring these values is one of the primary challenges in shoulder biomechanics. The shoulder contains multiple bones that need to be tracked for a complete description of its motion, and a substantial amount of movement is obscured by movement of the bones beneath the skin, which leads to inaccurate estimates of the joint angles. Researchers have attempted a variety of methods for measuring shoulder movements:

- static palpation of anatomical landmarks using traditional goniometers [126] or custom instruments [96, 98];
- roentgenography and fluoroscopy, with varying planes and marker methods [45, 52, 75];

- magnetic resonance imaging [101];
- videographic methods [63, 118]
- motion capture systems attached to bone pins [54, 70];
- non-invasive motion capture with surface markers [6, 18, 31, 66];
- custom fixtures that remain in contact during dynamic motions [54, 74];
- array of motion capture markers across the back for surface/tissue deformation [10, 108]; and
- conductive foam pressure sensors integrated into garments [24].

Most of these methods can be used to capture the complete motion of the shoulder complex, which simplifies data collection and processing. The last three methods are customized for scapular motion and can supplement the other methods. However, these techniques were insufficiently accurate [10], were inferior to non-invasive motion capture [54], or have not been adopted by other researchers.

Recent studies have primarily used non-invasive motion capture for valid dynamic measurements without the risk of long-term health effects from invasive or radiation-based methods. Although soft tissue artifacts are a common factor in marker-based studies, this issue is substantial on most areas of the scapula due to significant subdermal motion. Scapular sensors are commonly placed on or near the acromion to alleviate this, and accuracy can be further improved by using an empirical model of the skin motion [54] or multiple calibration points [12]. Shoulder motion can be estimated without any sensors by using regression equations from other studies, but these have generalization and accuracy issues [123]; these are discussed in more detail in Chapter 2.

Although the non-invasive methods have become the standard for measuring shoulder motion during dynamic movements, they cannot be applied to rehabilitation exoskeletons or spacesuits. The physical design of the exoskeleton often occludes optical motion capture, and the electromagnetic interference (EMI) of the motors reduce the accuracy from electromagnetic motion capture and IMUs. Also, the free space between the user's shoulder and the robot structure is often reduced to achieve lighter devices with smaller footprints, which limits the available space for skin-mounted sensors. Spacesuits share similar occlusion and EMI issues that exoskeletons experience, and skin-mounted sensors can both complicate donning the suit and increase crewmember discomfort if placed improperly. In addition, spacesuits must satisfy a wide variety of requirements (pressurization, radiation protection, operation in a high oxygen environment, etc.), so the suit hardware cannot be adapted to accommodate common sensing methods. So, a method for estimating shoulder girdle angles that uses more accessible measurements and can be applied to these complex cases of human-device interaction would allow for better recognition and response to abnormal shoulder motion.

1.5 Thesis Outline

Several shoulder measurement methods have been thoroughly developed and tested in biomechanics research, but they cannot be applied in certain settings. The few rehabilitation exoskeletons that support shoulder girdle movements have limited ability for shoulder girdle measurement, and their structure prevents the use of most measurement tools. Shoulder movement within existing EVA suits has similar measurement issues, and the numerous suit design objectives require assessment methods to accommodate the hardware. More invasive measurement methods cannot be used

in either population because of risk of infection, excessive radiation exposure, or other unacceptable complications. Shoulder regression models, which are discussed in detail in a later chapter, have limited generalization and accuracy when dealing with new testing conditions or subjects. Both exoskeletons and the EMU apply significant interaction forces on the user, which may lead to different kinematics when compared to the unloaded condition. A kinematic model of the shoulder that uses more accessible motion data to estimate shoulder configuration would expand the amount of information available for assessment and decision making.

This thesis details the development of a numerical model for estimating the configuration of the shoulder girdle (i.e., the orientation of the clavicle and scapula). This model should be applicable to a variety of arm movements and loading conditions without requiring a traditional suite of kinematic sensors. The model is designed to maintain kinematic closure at the synovial articulations while constraining the position of select scapula landmarks relative to the thorax. This should restrict the outputs of the model to realistic shoulder girdle configurations while remaining applicable to different subjects and experimental conditions.

Chapter 2 provides a summary on the different types of contemporary shoulder models as a background for the model developed in this thesis. Although these existing models are useful for areas such as robot design or musculoskeletal modeling, many assume sufficient generalization from a few types of motions or rely on full kinematic data as inputs. This prevents them from being used to describe the high-effort and occluded movements associated with exoskeletons and spacesuits.

Chapter 3 describes the development of a novel kinematic shoulder model. The model is scaled with subject anthropometry and uses kinematic information about

the torso and humerus (the proximal and distal bounds of the shoulder complex) as inputs. This information is applied to kinematic constraint equations from a mechanically similar spatial linkage to define the set of shoulder linkage angles that maintain kinematic closure. This solution set is used in a nonlinear optimization routine to find the linkage angles that maintain the desired distances between the scapula and the thorax.

Chapter 4 presents the results of this model when applied to an existing dataset from another research group [9]. The shoulder girdle angles and scapular landmark positions returned by the model are compared with this measured data. The sensitivity of the model is also tested for representative measurement variables and anthropometric parameters. The model is also compared with a selection of existing shoulder motion regression models to evaluate the relative accuracy and generalizability of this model to existing methods. Finally, a mixed effects model for the scapular landmark positions is developed and tested as an alternative to the ideal measures used in the preceding analysis, as these locations are difficult to measure dynamically.

Chapter 2

Review of Existing Shoulder Models

A variety of models have been developed to describe the complete motion of the shoulder complex. The most common types of these are regression models from experimental data, kinematic models, and musculoskeletal models. Regression models use experimental measurements to correlate other predictors, such as HT angles, to shoulder girdle angles. This is the only type of model capable of estimating clavicular and scapular angles without directly measuring them, which removes the need for direct measurement of shoulder girdle angles. Existing kinematic models use a complete set of shoulder joint angles to describe reachable workspace, estimate segment lengths, or calculate other movement quantities. Musculoskeletal models use segment kinematics to estimate biomechanics quantities that are difficult to measure, such as muscle forces and joint loads. An supplemental overview of these models is contained in [25].

2.1 Regression Models from Human Data

Regression models correlate humerothoracic angles and other anthropometric parameters to the other movements of the shoulder, typically the angles of the clavicle and scapula. These models are useful for estimating shoulder motion when typical measurement methods are impractical. This has led to their adoption in other areas of research, such as complex shoulder models or robotic devices [49, 90, 91].

Multiple research groups have put forward different regression models, each with their own input parameters and experimental protocol. The simplest regressions only use humerothoracic elevation as inputs [61, 87, 91], which requires the assumption of generalization across elevation planes. Some models used multiple regression equations for different planes of elevation [85,110], while others include the plane of elevation as an input parameter [39, 45]. The model proposed by de Groot and Brand includes the resting posture and direction of static arm loading, which is unique among regression models [19]. Later models have found anthropometric parameters to be significant contributors, even though earlier research did not find them significant [124].

One primary concern with using these regressions is generalization to different subjects and testing conditions. Xu et al. evaluated six different regression models with separate data from fourteen subjects and found none of the models to be clearly superior at predicting shoulder girdle angles [123]. In addition, although mean errors could be relatively low, the RMSE for all models and angles exceeded 6°, which is enough to risk clinical misinterpretation [71, 80]. Furthermore, these models do not consider kinematic closure of the shoulder or skin motion artifacts. The outputs of the model, while minimizing the error across subjects and motions, is not guaranteed to correctly position the humerus and remainder of the upper limb.

2.2 Kinematic Models of the Shoulder Complex

Kinematic models of the shoulder use joint constraints, anthropometry, and shoulder geometry to describe its motion. One of the earliest kinematic models for shoulder motion was presented by Dvir and Berme [26]. They described the shoulder

complex as a combination of spatial mechanisms: a closed kinematic chain containing the SC, AC, and ST joints; and an open kinematic chain containing the SC, AC, and GH joints. The general motion of the links are separated into different phases of elevation, relating bone movements to ligamentous restrictions and muscular activity. Even though this is a qualitative description of shoulder motion, the "two-mechanism" idea became a fundamental part of several future shoulder models.

Some of the shoulder models are focused on estimating the reachable workspace of the arm. Engin and Tümer presented a shoulder model using anatomical joint limits, also called joint sinus cones [32, 116]. These joint limits were derived by minimizing the individual joint angles needed to realize arm circumduction motions. This model was developed for designing manikins with physiologically similar joints and other computational models requiring range of motion data. Thus, the model cannot be applied to motions within the joint boundaries without adding several coordination behaviors among the multiple DOF. Klopčar et al. developed a model of the shoulder complex that avoids this limitation. The mobility of the shoulder girdle is simplified to the translation of the humeral head via two rotations and one translation. The model combines measured shoulder and elbow joint limits with this shoulder girdle motion to iteratively construct the reachable workspace of the wrist [62]. However, this model uses its own regression for shoulder girdle motion [61], which introduces the aforementioned generalization issues.

Bao and Willems proposed a kinematic model estimating the location of the shoulder joints from motion capture data [5]. The model used a "constant distance joint" to describe the constraint between AC and GH locations. However, the model focused on locating joint centers rather than joint angles, so the configuration of the

scapula is undetermined about the axis between the AC and GH joints. This model was only tested with a single subject and requires acromial motion measurements as an input.

Another group of kinematic models are intended to recreate shoulder motion in robotic systems. Roboticists have designed mechanisms that replicate the motion of the shoulder girdle in order to improve the capabilities of humanoid robots. These designs tend to fall into two groups according to their mechanical structure. The first of these use parallel mechanisms to reproduce the motion of the scapula, particularly the orientation of the glenoid [50, 67, 91]. An alternate method uses a serial RRP mechanism to reproduce the translation of the GH joint [114]. While these models may present alternatives for kinematic descriptions and motion planning [51], the lack of anatomic joint angles hinders their adoption for biomechanics studies.

Two of the most recent kinematic shoulder models are used to improve the compatibility of measured data with biomechanical models. Bolsterlee et al. proposed optimizing with "soft constraints" to balance possible conflict between marker data and kinematic constraints [9]. This optimization procedure still favors the measured data while preventing issues like soft tissue artifact from predicting unrealistic ST distances or excessive conoid ligament strain. This method was able to substantially reduce changes in input joint angles used by a musculoskeletal model with only small deviations from constraint conditions. Seth et al. created an OpenSim [21] shoulder model component for refining marker data collected during motion studies (Figure 2.1) [109]. This type of model is commonly used in lower limb studies for reducing the impact of soft tissue artifacts on motion capture data before running musculoskeletal simulations (e.g., [69]). Both models also allow for scapular winging to occur, which

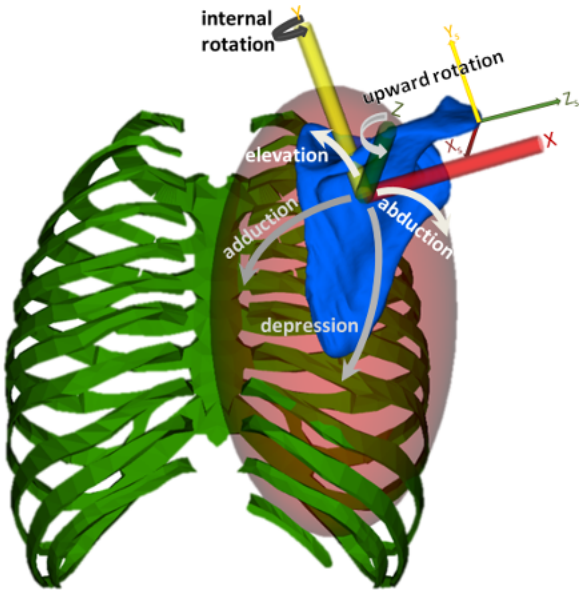

Figure 2.1: Visual representation of the OpenSim ST joint model. Reprinted with permission from [109].

allows them to be applied more readily to patient populations with abnormal scapular stability. However, the models require measurements of ST angles, making them difficult to use when traditional shoulder measurement methods are not viable.

2.3 Musculoskeletal Models of the Shoulder Complex

The final type of models for the shoulder complex are musculoskeletal models. These have emerged in the past few decades and have distinguished themselves from kinematic models by the types of questions they can address. For example, inverse dynamic simulations with these models use segment motion data and external forces to estimate the internal muscle and joint forces during a movement[1]. Due to the

[1]Forward dynamic simulations, which use muscle forces or neural input to predict skeletal motion, are not covered here because estimating these quantities is a daunting task for the shoulder complex (see Section 1.1).

complex properties and arrangement of the neuromuscular system, many biomechanics and rehabilitation questions, such as muscle forces during an arm movement or effects of different gait treatments [21], cannot be addressed without modeling these elements. This section provides a brief overview of the design and purpose of several musculoskeletal models for the shoulder. For a more thorough review of the more prominent arm and shoulder models, see Bolsterlee et al. [8].

One of the more prominent models is the Delft Shoulder and Elbow Model (DSEM), and its initial development as a finite element model began in the 1980's [117]. The model predicts muscle and joint forces from shoulder kinematic data and external loads and includes axioscapular muscles to drive the scapula. It was also the first musculoskeletal shoulder model to include ST gliding constraints for constraining the medial border of the scapula. Example applications of this model include shoulder muscle forces during arm elevation [40] and wheelchair propulsion efficiency [11].

The other most widely used model is the MoBL-ARMS model, which focuses more on the distal joints of the upper extremity [49, 106]. Muscle routing for these muscles was adjusted to best match the moment arms from experimental data. Although this model lacks axioscapular muscles, it includes muscles for the wrist and hand. This model also uses a simplified version of the regression model by de Groot and Brand [19] to define the motion of the shoulder girdle in terms of humeral elevation. This model has been used to address research questions on muscle transfer surgeries and wheelchair propulsion [33, 99].

Several other musculoskeletal models have been developed over the years to answer similar questions (e.g., [7,14,23,37,44,78,121]). Some of these, particularly the MoBL-ARMS model, use the aforementioned regression models to estimate unmea-

sured scapular motion. Other models, such as the DSEM or Maurel models, require measured shoulder girdle data as part of the kinematic inputs. Each of these has their own limitations when considering model accuracy and shoulder girdle behavior. Models that directly use measured shoulder kinematics, such as DSEM, can return significantly differences in some of the muscle forces with small changes in the kinematic data [9]. This means that highly accurate shoulder angles and joint models are needed for some analyses, which is difficult to collect and implement. On the other hand, models that rely on regression techniques take on the same issues of applicability to other experiments. Richardson et al. found errors greater than 10° between their measured data and the coordination pattern prescribed by the MoBL-ARMS model [102]. Considering the impact that small angle changes had on the outputs of DSEM, it could be expected that the regression models would produce larger errors for muscle forces and other quantities around the GH joint.

2.4 Modeling Scapulothoracic Interaction

One feature common to several of these models is the scapulothoracic gliding (STG) surface which applies constraints to the medial border of the scapula [97]. This is usually interpreted as constraints on the behavior of two scapular landmarks: the root of the spine of scapula (trigonum scapula, TS) and the inferior angle (angulus inferior, AI). This method has been used to restrict both the kinematics and dynamics of several shoulder models.

Some models use this constraint to affix the landmarks to the surface of the thorax [36, 51, 110]. Using this as a kinematic constraint requires either measurement of the distances between the landmarks and the ribcage or assuming constant values.

But, recent research has shown that using fixed distances from the ellipsoid can have significant effects on predicted muscle forces [9]. The OpenSim joint model represents a partial implementation of this restriction, since it allows for variable scapular winging while keeping the vertical axis of the scapular reference frame tangent to the ribcage [109].

Most musculoskeletal models use the STG constraint to restrict the predicted muscle forces models so that the forces between the scapula and ribcage are only compressive [117]. This allows for the scapula to wing from the ribcage so long as the axioscapular muscles are working to reduce this distance. However, without correcting the kinematic data for skin motion artifacts or other issues, the musculoskeletal models will attempt to follow the kinematic data, which can result in excessive winging under certain conditions. A similar, opposing method can be implemented to keep the scapula from intersecting the ribs if excessive correction is applied [46].

Both forms of the STG constraint need the geometry of the ribcage to ensure the distances and force directions are proper. For simplicity, the gliding surface is approximated as a simple geometric volume with dimensions corresponding to the size of the ribcage. One musculoskeletal model treats this surface as a cylinder [46], but most other have used ellipsoids. The DSEM model uses a single ellipsoid for the entire thorax [117], while other models use one ellipsoid for each lateral half of the ribcage [36, 109, 110] or even one per contact point [51].

2.5 Summary of Shoulder Models

Numerous models have been proposed to represent the movement of the shoulder complex. Most biomechanics work uses motion capture data and a combination of

joint models to determine conventional anatomic joint angles. The regression models use this data to directly model movement behaviors, but extrapolating these models to other motions is not guaranteed to remain accurate. The kinematic models developed thus far have been designed to solve for different purposes, such as workspace of the arm or equivalent designs for humanoid robots. Musculoskeletal models require a complete set of kinematic data for simulating limb dynamics and neural control. Both kinematic and musculoskeletal models use shoulder girdle angles as inputs and often resort to regression models when these quantities cannot be consistently measured. None of the models that infer shoulder girdle angles use both kinematic closure of the serial shoulder chain and ST constraints of the parallel shoulder chain. A model with all of these features should be capable of consistently estimating feasible shoulder girdle angles without sensors on the clavicle or acromion. This would allow for clavicular and scapular angles to be estimated in complex environments that preclude the use of normal measurement methods, such as robotic exoskeletons and spacesuits.

Chapter 3

Shoulder Model Development

With the essentials of shoulder biomechanics presented and the contributions of other modeling efforts summarized, a new kinematic model can be developed with proper context. In this chapter, we present a new model for estimating clavicle and scapula angles without traditional shoulder measurement methods. The model should also respect geometric constraints at the joints by maintaining kinematic closure during shoulder motion. This restriction is enforced by using constraint equations from an analogous spatial mechanism to define the two internal DOF of the shoulder linkage.

3.1 Model Coordinates, Parameters, and Inputs

This model uses the joint angle convention proposed by the International Society of Biomechanics (ISB) [122], which has seen widespread adoption in academic research. Each bone of the right shoulder and arm is assigned a right-handed coordinate frame according to the position of skeletal landmarks. Three rotations are defined relative to parent frames on proximal segments according to Cardan or Euler angle sequences. By assuming that the joints have negligible translation of the rotation centers in these frames, these articulations can be treated as mechanical spherical joints. Scapula and humerus rotations can also be defined relative to the thorax using the same rotation sequence as their single-joint counterparts. The ST and humerotho-

racic (HT) rotations are both easier to visualize and avoid measurement difficulties with SC angles.

After defining the coordinates to describe the configuration of the shoulder, skeletal lengths are used to scale the model geometry. These lengths, along with other anthropometric measures, were provided with the kinematic data used to test this model[1] [9]. The long axis of the clavicle was defined between the SC and AC joint centers rather than the corresponding joint landmarks for more direct transfer to the kinematic model. Although the orientation of the clavicle is traditionally defined by the bony landmarks near these joints, it is assumed that this change has a negligible impact on the output angles.

Some of the scapular lengths are shared with the landmarks used to define the reference frames, but the distance between the AC and GH joints cannot be measured externally without medical imaging. In this thesis, the position of the humeral head is determined using standard forward kinematics with measured shoulder joint angles. It should be noted that this uses measured SC and ST angles, even though these would not be available in some circumstances and are, in fact, the desired outputs of the model. This is because significant errors were observed in the provided data. During initial testing, the humeral head location translated significantly in the scapular frame, even to the point of what would be considered traumatic joint dislocation. Since this position is critical to the model, this data was substituted with the forward kinematics estimate. The position of the GH joint center was estimated by scaling the joint position from the SIMM implementation of the Delft Shoulder and Elbow

[1]Certain measurements with abnormal values, such as SC joint centers located contralaterally, were assumed to only require a sign change to be correct.

Model [7, 60]. This scaling used the positions of the dorsal edge of the acromion, the root of the scapular spine, and the inferior angle of the scapula relative to the AC joint to create the scaling matrices used in [76].

3.2 Constraining Acromioclavicular Joint Location with RRSS Linkage Analysis

By using purely rotational joints, the shoulder girdle contains six rotational DOF. The position of the humeral head relative to the thorax is obtained from the measured positions and angles of the torso and humerus, constraining the scapula to rotate around the center of the GH joint. This is the same behavior described by Bao and Willems as a constant distance joint [5], and removes three DOF from the system. In addition, ignoring the axial rotation of the clavicle removes an additional DOF. This simplified shoulder complex has two kinematic DOF for orienting the scapula about the humeral head. This matches with previous analyses of shoulder girdle mobility for developing robotic analogues [67, 114].

The resulting arrangement of joints comprises two proximal, intersecting revolute joints for the simplified SC joint and two distal spherical joints for the AC and GH joints. This joint structure matches that of an RRSS spatial linkage [111, 112]. Several kinematicians have developed methods and equations for describing the mobility of this type of linkage, such as constraints on coupling between the revolute joints to maintain kinematic closure [113, 120]. Since the position of the humeral head is considered a known quantity, the shoulder girdle shares the same mobility constraints as this linkage. So, for a known position of the GH joint, RRSS linkage analysis techniques should be applicable for determining the mobility of the shoulder girdle and contribute towards defining the set of kinematically valid skeletal angles.

If this hypothesis is correct, measured shoulder girdle angles from typical biomechanics datasets should fall within this solution set. The exact location of the measured data would depend on subject anthropometry, joint properties, and the task being performed.

The linkage mobility equations define the angle limits for the two revolute joints, which control the movement of the input and coupler links. In this shoulder model, these two angles, θ and ϕ, are considered to the protraction-retraction and elevation-depression of the SC joint, respectively. These joint angles are considered to have intersecting axes, so the length of the input link (length a in [113]) is reduced to zero. These joint axes are also perpendicular to each other, which sets the input link twist angle α to 90°. In addition, since the coordinate frame of the clavicle is oriented from the SC joint to the AC joint, the distance along the coupler rotation axis q is also zero. The position of the humeral head in the thoracic frame is adjusted to be located relative to the SC joint to match the origin of the RRSS analysis. Then, the transverse distances between the two joints (x- and z-axes in the ISB convention) are combined to orient the x-axis of the linkage ground coordinate system from the SC joint towards the GH joint with an offset angle θ_0. The remaining lengths b, h, r, and p correspond to the length of the clavicle, length of the scapula between the AC and GH joints, transverse distance to the GH joint, and vertical distance to the GH joint, respectively. Figure 3.1 shows the geometric similarities between the RRSS linkage and the shoulder girdle. The simplified constraint equation for kinematic closure is given by Equation 3.1.

$$-2brcos(\theta)cos(\phi) - 2bpsin(\phi) + b^2 - h^2 + p^2 + r^2 = 0 \tag{3.1}$$

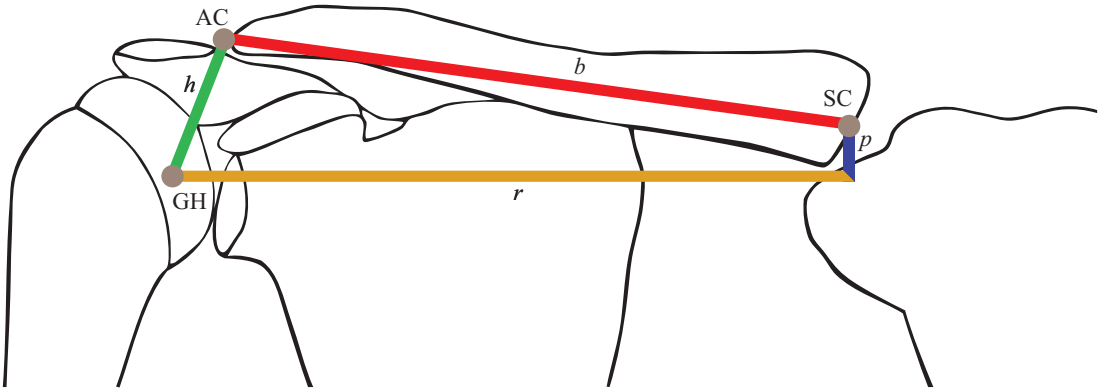

Figure 3.1: Shoulder girdle skeleton represented as an RRSS linkage. The SC joint is a pair of intersecting revolute joints, and both the AC and GH joints are spherical joints. RRSS parameters a, q, and α are zero in this model. r refers to the total transverse distance to the GH joint, not its projection onto the frontal plane. Reference image courtesy of Visible Body.

Similar limit polynomials can be derived for both the input and coupler angles; this work solves for the constrain equations in terms of input angle θ. By following the same derivation process as [113], one can arrive at biquadratic polynomial (i.e., a quartic polynomial without odd powers of x) after using a tangent half-angle substitution in θ:

$$m_4 x^4 + m_2 x^2 + m_0 = 0 \tag{3.2}$$

$$m_4 = 4b^2p^2 + 4b^2r^2 - (-b^2 + h^2 - p^2 - r^2)^2 \tag{3.3}$$

$$m_2 = 8b^2p^2 - 8b^2r^2 - 2(b^2 - h^2 + p^2 + r^2)^2 \tag{3.4}$$

$$m_0 = 4b^2p^2 + 4b^2r^2 - (b^2 - h^2 + p^2 + r^2)^2 \tag{3.5}$$

The roots of Equation 3.2 define the limits of movement for the input angle that maintain kinematic closure. In order to determine the joint angle limits, the classification of the linkage must be known. This classification is defined with the signs of the discriminants of the Sylvester matrix [125]. Su et al. present a set of sign

conditions that describes the behavior of the mechanism with regards to the mobility of the input link [113]. This determines how these input angle roots should be used when defining the domain of valid input angles.

For the shoulder, this classification depends on the subject's anthropometry and the relative position of the humeral head. Since linkage lengths could be expected to be reasonably bounded, both in absolute measurements and relative length ratios, the linkage type of the human shoulder could be expected to only fall into a subset of possible root cases and linkage types. Intuitively, the human shoulder could be expected to represent a double rocker mechanism, as the ratio of clavicle and scapula lengths would prevent the SC joint from performing a full revolution while maintaining kinematic closure. In addition, due to the numerical precision required for repeated roots to occur, the input angle could be expected to only have unique roots. This leaves configurations with two or four real roots as expected outcomes. The model assumes the input linkage mobility has four real roots when selecting bounds for θ and chooses the two angles closest to zero. This validity of this method is tested in Chapter 4.

Once the roots for θ are obtained, the range of the coupler angle ϕ can be evaluated. Algebraic manipulation of Equation 3.1 gives the following equation for ϕ as a function of θ:

$$\phi(\theta) = arctan\left(\frac{p}{rcos(\theta)}\right) \pm arccos\left(\frac{(-b^2 + h^2 - p^2 - r^2)}{\sqrt{4b^2p^2 + 4b^2r^2cos^2(\theta)}}\right) \tag{3.6}$$

Since these two angles are not independent, they can be reduced to a single DOF. For example, this could be reduced to a polar coordinate form in θ-ϕ space as a

phase angle ζ and radius $\rho(\zeta)$. However, this would result in a dependency on ζ that is complicated to implement, particularly for online monitoring and control or repeated calculations during an optimization process. An approximate representation of the θ-ϕ curve would ease implementation of this kinematic constraint in other elements of the shoulder model.

Fortunately, this curve can be simplified significantly by reducing it to an ellipse in θ-ϕ space. In this approximation, the θ roots define the first axis of the ellipse and are nearly equidistant to $\theta = 0°$. Since the ellipse is horizontally centered, the ϕ-axis and center can be defined by evaluating Equation 3.6 as $\phi(\theta = 0°)$. Since the input angle is defined such that the line from the SC joint to the GH joint is equivalent to $\theta = 0°$, the offset θ_0 is used to adjust the center of the ellipse to match the ISB convention. The resulting approximation for the ISB angles are given in Equations 3.7 and 3.8, with sign changes to account for coordinate differences between the RRSS and ISB frames for the right shoulder. ϕ_0 is the vertical offset of the ellipse, and ρ_i are the radii for each axis of the ellipse. At the instant described by Figure 3.2, the error between the two is visually indiscernible. Closer inspection reveals increased error near the limits of θ where ζ is a multiple of 180°. This error resulting from this approximation is tested on a larger dataset in Chapter 4.

$$SC_Y(\zeta) = \theta_0 + \theta_{RRSS} \approx \theta_0 + \rho_\theta cos(\zeta) \tag{3.7}$$

$$SC_X(\zeta) = -\phi_{RRSS} \approx -\phi_0 - \rho_\phi sin(\zeta) \tag{3.8}$$

It is important to understand what this ellipse means, or, more importantly, what it does not describe. This curve does not represent the range of motion of any articulation in the shoulder complex. The most likely confusion is that this curve

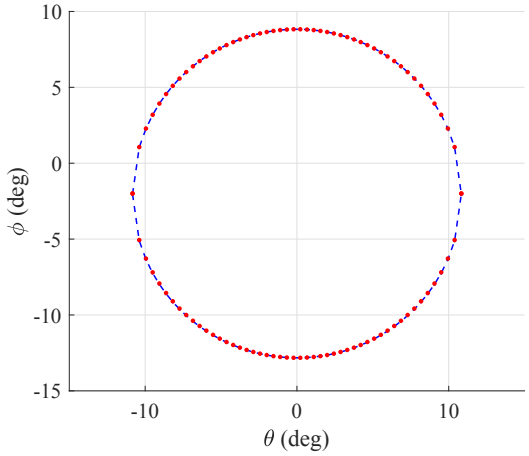

Figure 3.2: Comparison of θ-ϕ solution curve with ellipse approximation at a single instant for a selected subject and motion. The blue dashed line is the solution from Equation 3.6, and the red dots are from Equations 3.7 and 3.8.

represents the range of motion of the SC joint. This is likely a matter of habit, since joint mobility typically describes the bounds of a joint's range of motion with parameters similar to the axis lengths of Figure 3.2. In addition, the joint sinus cone for the SC joint is relatively elliptical for varying levels of force [22]. However, those measures describe the loading properties of the joint capsule and other tissues that could be realized during maximal shoulder motions. In contrast, the joint space curve of Figure 3.2 shows the mobility of the shoulder girdle mechanism for a known position of the humeral head. In other words, if the ligaments and other tissues were removed but the joints were kept congruent, the shoulder girdle would remain a closed kinematic chain for any point (θ_i, ϕ_i) selected from this curve.

3.3 Optimization of Linkage Angles for Scapulothoracic Contact

Although the ellipse for SC joint mobility constrains the range of possible joint angles, it is not sufficient for fully defining the configuration shoulder girdle. A second degree of freedom is located between the AC and GH joints that is not constrained by the input and coupler links of the RRSS linkage. The axial rotation of segment h in Figure 3.1, defined as η, would be a passive DOF in mechanical linkages to prevent binding. However, this angle in the human shoulder is needed for proper orientation of the scapula and proper ST interaction. This angle does not correspond to any rotation of the ISB convention (rather, portions of the rotations about each axis), and the orientation of the rotation axis depends on the value of the SC joint angles.

The rotation axis for η must pass through the GH joint in order to maintain kinematic closure. This requires rotating from the body-fixed frame of the clavicle about an arbitrary axis. The intermediate rotation angle γ and axis u_γ can be found using Equations 3.9-3.11:

$$\gamma = arccos\left({}^{ST3}u_{AC}^{GH} \cdot {}^{ST2}u_{AC}^{GH}(\zeta)\right) \tag{3.9}$$

$$\begin{bmatrix} {}^{ST2}p_{AC}^{GH} \\ 1 \end{bmatrix} = \begin{bmatrix} R_{ST0}^{ST2}(\zeta) & {}^{ST2}p_{AC}^{SC} \\ 0 & 1 \end{bmatrix} \begin{bmatrix} {}^{ST0}p_{SC}^{GH} \\ 1 \end{bmatrix} \tag{3.10}$$

$$u_\gamma = {}^{ST3}u_{AC}^{GH} \times {}^{ST2}u_{AC}^{GH} \tag{3.11}$$

${}^{A}p_{C}^{B}$ is the position vector from point C to point B in reference frame A; the same convection applied for unit vector u. R_S^Q represents the rotation matrix from frame S to frame Q. *ST0* is equivalent to the thoracic frame, *ST2* is the frame fixed to the clavicle (neglecting its axial rotation), and *ST3* is the intermediate frame for the axial rotation γ. The rotation between the *ST0* and *ST2* frames encapsulates

the SC joint angles, making the transformation matrix a univariate function of ζ. Although the orientation of the rotation axis in the *ST3* frame can be set arbitrarily, defining it to be parallel to the vector from the AC joint to the GH joint in the ISB scapular frame simplifies later calculations.

These rotation parameters are used to construct a rotation matrix about u_γ that is only a function of ζ. These transformations can be used locating scapular landmarks in the thoracic frame in terms of the the shoulder linkage angles ζ and η:

$$\begin{bmatrix} {}^{ST0}p_{IJ}^{Q} \\ 1 \end{bmatrix} = T_{ST2}^{ST0}(\zeta) T_{ST3}^{ST2}(\gamma(\zeta)) T_{ST4}^{ST3}(\eta) \begin{bmatrix} {}^{ST4}p_{AC}^{Q} \\ 1 \end{bmatrix} \tag{3.12}$$

where IJ refers to the intrajugular landmark (the origin of the thoracic frame) and Q refers to any scapular landmark.

To solve for ζ and η, two additional equations are needed. This model uses two distance constraints on landmarks of the medial border of the scapula, the root of the spine of the scapula (TS) and inferior angle (AI), from the ribcage. These points are assumed to be some distance away from an ellipsoid, which approximates the shape of the ribcage. These values were part of the provided dataset [9], and it was assumed that respiration or any movement of the spine has negligible change on its geometry. In this model, the distances between the two landmarks and the STG ellipsoid are assumed to be known at each instant. This results in the constraint equations of the following form:

$$\| {}^{ST0}p_{IJ}^{Q} - {}^{ST0}\, p_{IJ}^{Q_E} \|_2 = d_Q \tag{3.13}$$

where Q is landmark TS or AI, Q_E is the projection of the landmark onto the ellipsoid, and d_Q is the STG distance for landmark Q. These distance can vary over time and are difficult to measure, and the methods for estimating these distances during analysis

are described in Chapter 4. The projected point Q_E was determined by a numerical optimization algorithm for projecting points onto a hyperellipsoid [28].

With Equations 3.12 and 3.13, the linkage angles ζ and η can be solved for. However, this must be done numerically for two reasons. First, it is impractical to symbolically invert Equation 3.12 to solve for the unknown angles. Second, the ellipsoid projection method uses its own numerical root finding method for finding the nearest point on the ellipsoid, which prevents this equation from being represented and inverted analytically. Thus, a nonlinear least-squares optimization routine in MATLAB (The MathWorks, Inc., Natick, MA, USA) is used to find the linkage angles that minimize the error vector ϵ:

$$\min_{\psi} = \|\epsilon(\psi)\|_2^2 \tag{3.14}$$

$$\epsilon = \begin{bmatrix} d_{TS}(\psi) \\ d_{AI}(\psi) \end{bmatrix} - \begin{bmatrix} \delta_{TS} \\ \delta_{AI} \end{bmatrix} \tag{3.15}$$

where ψ is the vector of linkage angles (ζ, η), and δ_Q is the desired distance between the landmark Q and the STG ellipsoid. Minimizing ϵ results in shoulder linkage angles that satisfy the STG distance constraints and maintain kinematic closure of the shoulder girdle.

This minimization can encounter multiple minima in ζ-η space that would place the TS and AI landmarks at appropriate distances from the ellipsoid. These can be obtained by repeating the optimization over a set of initialization points using nearby shoulder linkage angles. However, some of these solutions are physiologically infeasible and place the scapula on the anterior surface of the ellipsoid or vertically invert the scapula. These positions are rejected by constraining the landmarks as follows:

- Both landmarks must remain on the posterior surface of the ellipsoid within a small margin of error[2];
- The AI landmark must remain caudal to the TS landmark since the scapula does not experience more than 90° of upward rotation relative to the torso; and
- Both landmarks must not cross the medial plane, as the scapula does not overlap the spine.

After culling any solutions that result in infeasible shoulder configurations, there are typically two solutions remaining. One of these generally has smaller shoulder linkage angles and corresponds to less scapular upward rotation. The second of these has larger shoulder linkage angles and indicates a more elevated shoulder girdle. Yet, both of these obtain the same STG distances and humeral head position. The positions of these solutions move in ζ-η space according to the STG distances and translation of the GH joint. In addition, during most elevation tasks, these solutions converge towards a single point between them at certain shoulder configurations. As the motion continues, these points diverge from each other. An example of the two solutions in ζ-η space is shown in Figure 3.3. The dotted lines represent contours that match the desired distance for the corresponding scapular landmark. Both solutions occur at local minima of Equation 3.14 and match the intersections of the individual contours for TS and AI distance solutions.

The primary issue with this pair of solutions is that the correct solution switches between the smaller and larger pairs at the point of minimum separation. If only one of these solutions was chosen consistently, the scapula would rotate in an

[2]The AI landmark may cross the Y-Z plane of the STG ellipsoid by a couple centimeters at high elevation angles, so this constraint must be relaxed.

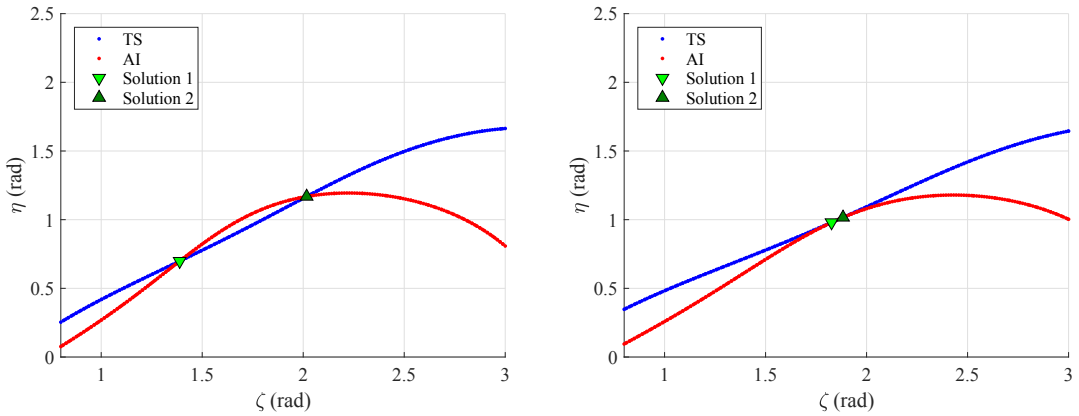

Figure 3.3: Example contour plots of each scapulothoracic gliding distance and linkage angle solutions for a selected abduction motion. (a) Solutions at a low shoulder elevation angle are noticeably separated. (b) Solutions at a higher elevation configuration approach the minimum distance point.

unexpected manner during arm elevation. For example, if only the smaller solution was used, the scapula would rotate upward normally until the two solutions reached their minimum distance. By continuing to elevate, the solutions would move apart, and the lower solution would slowly increase (or even decrease) in ζ and η. This would be perceived as a restriction on scapular upward rotation during humeral elevation, which would result in an increased risk of shoulder impingement. So, a more involved method is needed to choose between the linkage angle solutions.

The choice between the two linkage solutions is made using the two predictions for scapular upward rotation, one of the resulting shoulder girdle angles. First, both the difference between the two angles (δ) and the direction of humeral elevation are causally smoothed with low-pass Butterworth filters. Then, a backwards window of past δ values are used to determine if a local minimum has occurred. These minima can occur if shoulder girdle motion changes direction or if the minimum distance

configuration is passed through. If the shoulder is approaching the minimum distance point from a state of lower elevation, continued elevation would result in further decreases to this distance, while changing movement direction would create a local minima. The opposite behavior is seen when elevated beyond the minimum distance point—lowering the shoulder decreases the distance, and vice versa. So, using the direction of arm elevation[3] and the distance between possible solutions should be sufficient to successfully switch between sets of linkage angles in nearly all cases.

If a local minimum is found and its value is less than a specified threshold, the elevation direction is used to choose between them. If the arm was elevating when the minimum occurred, the solution with the larger ζ is chosen. If the arm was lowering, the solution with the smaller ζ is chosen. The threshold used for this is determined manually for each subject by using data such as Figure 3.4. For example, the angle threshold would need to be at least 2° for switching to occur during this motion. If no minimum is found or the minimum value exceeds the threshold, the solution decision from the previous iteration is maintained. For initialization, the algorithm assumes that the arm starts in a lowered position and automatically selected the smaller solution. A flow chart representing this process is shown in Figure 3.5. It should be noted that this introduces a dependence on movement velocity, and changes the model type from purely geometric to kinematic. This adds a requirement of using sufficiently continuous motion data, as large jumps from sensor dropout or other issues can lead to incorrect solution selection.

[3]Although using the elevation angle of the humerus assumes that any independent shoulder girdle motion does not oppose SHR, this is acceptable for the range of motion and functional movement data studied in Chapter 4.

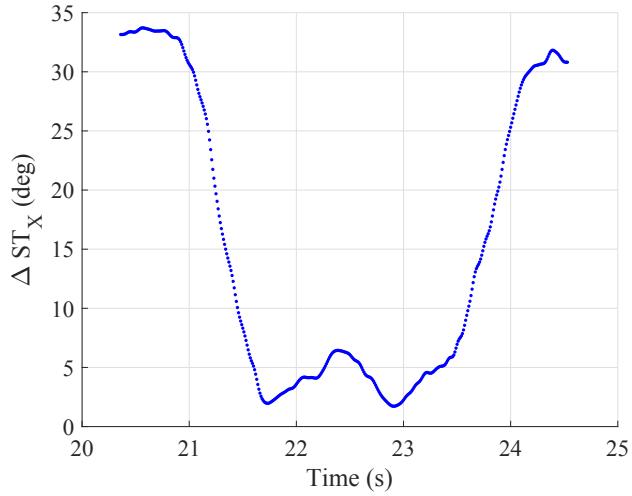

Figure 3.4: Filtered solution switching variable (scapular upward rotation) for an example abduction motion.

When solving for the linkage angles, Equation 3.15 depends on subject anthropometry, the position and orientation of both the torso and humerus, the STG distances, and the direction of arm elevation. Once this equation is minimized, the scapular landmark positions can be found with forward kinematics using Equation 3.12. These landmark positions define the orientation of the scapula with respect to the thorax, and this rotation matrix is used to find the ST angles. The linkage angle ζ locates the clavicle within its solution space and defines the SC angles via Equations 3.7 and 3.8.

3.4 Summary of Model Development

This model uses the similarities between the shoulder girdle and an RRSS spatial mechanism to estimate the configuration of the scapula and clavicle relative to the thorax. Since this linkage is a 2-DOF system, two STG distance constraints are needed to fully define its configuration. A numerical optimization is used to solve the

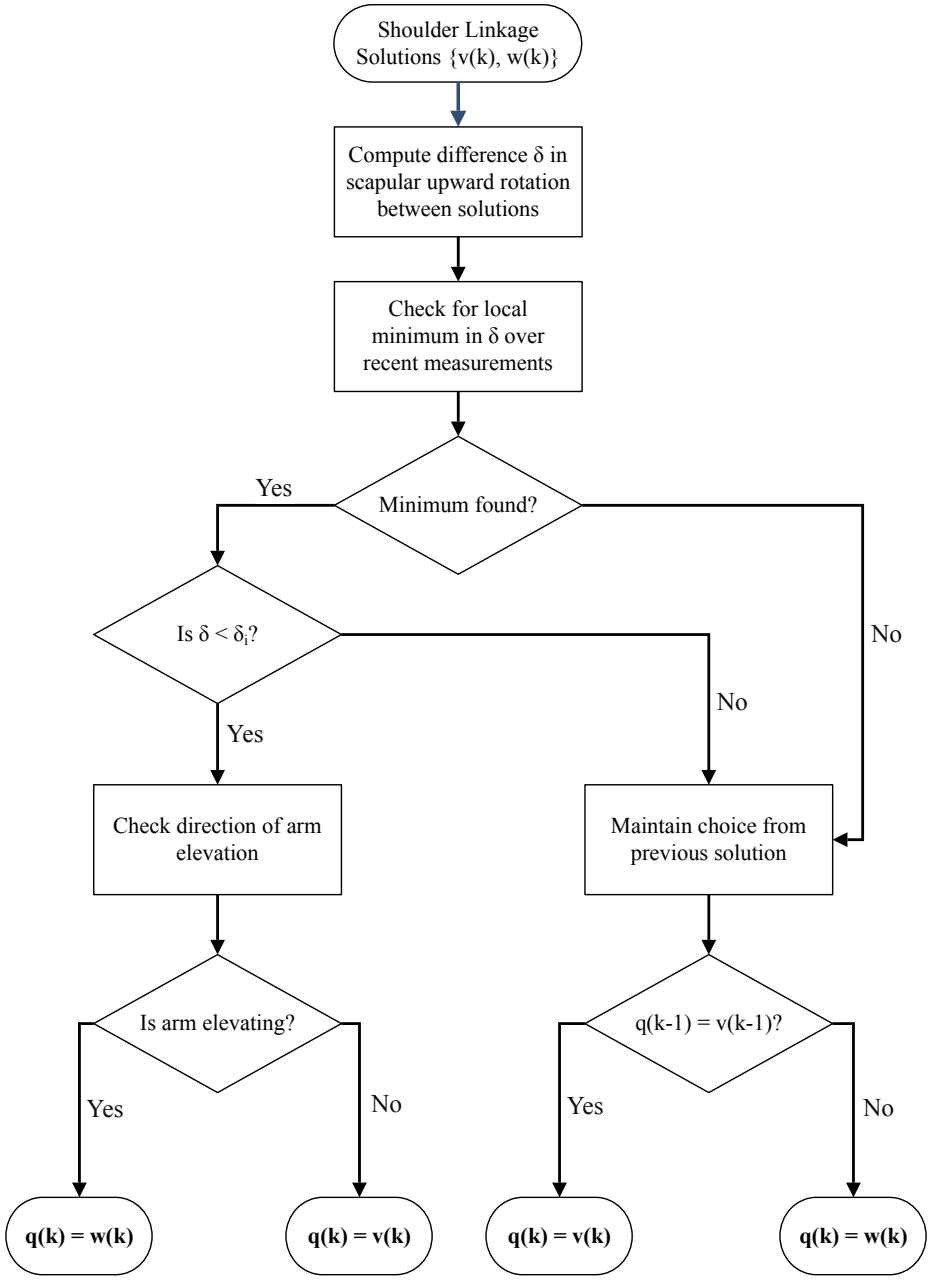

Figure 3.5: Flowchart of the optimization solution selection process. $v(k)$ and $w(k)$ are the two solutions returned from the optimization at step k, and $q(k)$ is the selected solution. δ_i is the switching threshold for subject i. At the first time step, the arm is assumed to be in a lowered orientation ($q(1) = v(1)$).

complex relationship between shoulder linkage angles and STG distances. One viable shoulder configuration is selected from the two optimization solutions according to the direction of humeral elevation and the distance between the solutions. If the STG distances are known, the model can be applied to any movement of the arm, regardless of movement speed, direction, or loading. These advantages should result in improved shoulder girdle estimation during interaction with complex environments relative to regression models.

To develop this model, several assumptions had to be made at various stages of the development process. These assumptions are listed below:

- joints have negligible translation and rotate about intersecting axes;
- SC and AC joint centers are suitable analogues for the SC and AC bony landmarks;
- the set of RRSS linkage input and coupler angles can be reduced to an ellipse with sufficient accuracy;
- scaling of scapula geometry between subjects and the reference cadaver model allows for adequate estimation of the vector between AC and GH joint centers; and
- STG distances are known or can be estimated to solve the nonlinear optimization.

So, this model relies on accurate measurement of anthropometrics and arm kinematics as well as valid assumptions about joint behavior and ST modeling. The validation of this model, including sensitivity analysis, is described in the next chapter and evaluates both the validity of this overall approach and its reliance on these assumptions.

Chapter 4

Shoulder Model Evaluation

The model developed in the previous chapter is designed to estimate the shoulder girdle angles using anthropometry and kinematics of the torso and humerus. This development included assumptions about joint behavior, simplifications in the linkage angle constraints, and unintuitive elements in the selection between optimization solutions. These complexities could introduce conditions or edge cases that result in improper prediction of shoulder girdle angles. So, model performance must be evaluated thoroughly to establish possible limitations. This is done by assessing model performance under both ideal conditions and after perturbing certain parameters or inputs. In addition, the linkage model must be compared with existing regression models to justify the extra complexity in implementation. If the linkage model is robust to measurement noise and outperforms the existing regressions, then it can be recommended for future studies of shoulder biomechanics.

The movement data used for this evaluation was collected and processed by another research group for shoulder modeling research [9]. This anonymized data includes motions for five healthy subjects performing a variety of range of motion movements and tasks representing activities of daily living. Since the solution selection process requires relatively continuous data (Figure 3.5), movements with significant gaps in any shoulder angle were dropped from the analysis. The remaining motions were trimmed to single movement repetitions for computational ease. This resulted in

77 movement sets to validate the model. Before testing, the measured data was processed according to the "soft constraints" kinematic optimization method [9], which adjusts surface marker data to discourage unrealistic STG distances.

4.1 Model Validation

The baseline model evaluation consists of measuring the error between measured shoulder girdle angles and model outputs. To confirm that the model can produce accurate results in a reliable manner, this process is split into two primary elements. The first portion deals with evaluating the behavior of the RRSS linkage equations, which constitute a novel addition for shoulder modeling. The second portion focuses on the model outputs from the optimization and solution selection. This ensures that each element of the model is operating correctly before performing other analyses.

4.1.1 RRSS Model

The first validation of the RRSS method checked the consistency of the linkage classification. Knowing how the linkage class changes during arm motion is critical for calculating the input and coupler angle domains. During development, it was initially assumed that the linkage input angle had four real roots. From the analysis by Su et al., two of these should lie on either side of 0°, while the other two should similarly surround 180° [113]. This was tested by calculating the discriminants of the resultant matrix for Equation 3.2 over an array of humeral head positions for each subject. Since the linkage lengths are constant during the motions, any change in the roots of Equation 3.2 would be due to translation of the GH joint relative to the SC joint.

This testing showed that the shoulder linkage was represented by only two cases. When humeral head positions are significantly close or far away from the SC joint, the linkage fails to maintain kinematic closure and has no roots for the input angle θ. At intermediate positions, θ has four real roots that limit its domain, with two of them outside the feasible range of the SC joint. This leaves two roots to define the maximum and minimum values for θ. A set of example contour plots and polynomial discriminant values for humeral abduction in one subject is shown in Figures 4.1 and 4.2. The humeral head position always remains in a region where the discriminants $\Delta_2 - \Delta_4$ are positive, confirming that the linkage has four real, unique roots throughout the motion. Even though the position of the humeral head moved towards to the edges of this region in other cases, this behavior was maintained for all motions and subjects tested.

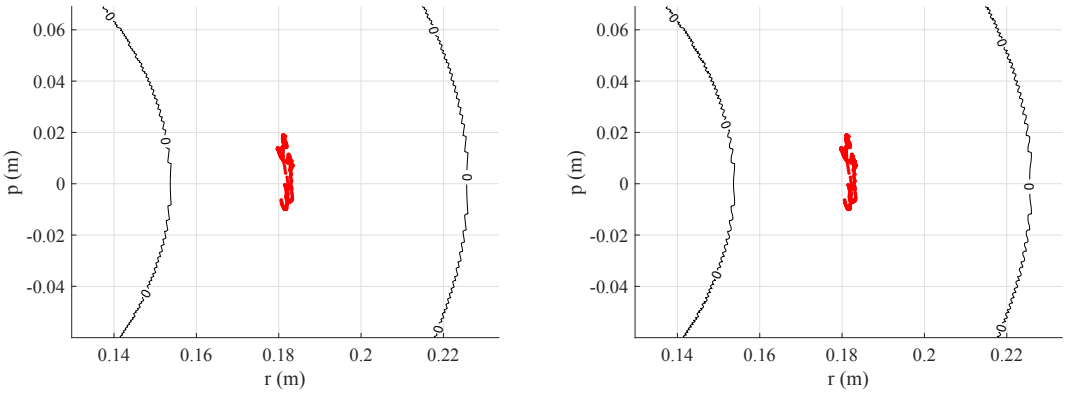

Figure 4.1: Contours of resultant matrix discriminants Δ_2 (a) and Δ_3 (b) over humeral positions r and p. Red dots identifies the location of the GH joint center during an example abduction motion. Δ_4 remains positive over all simulated locations of the humeral head and is not shown.

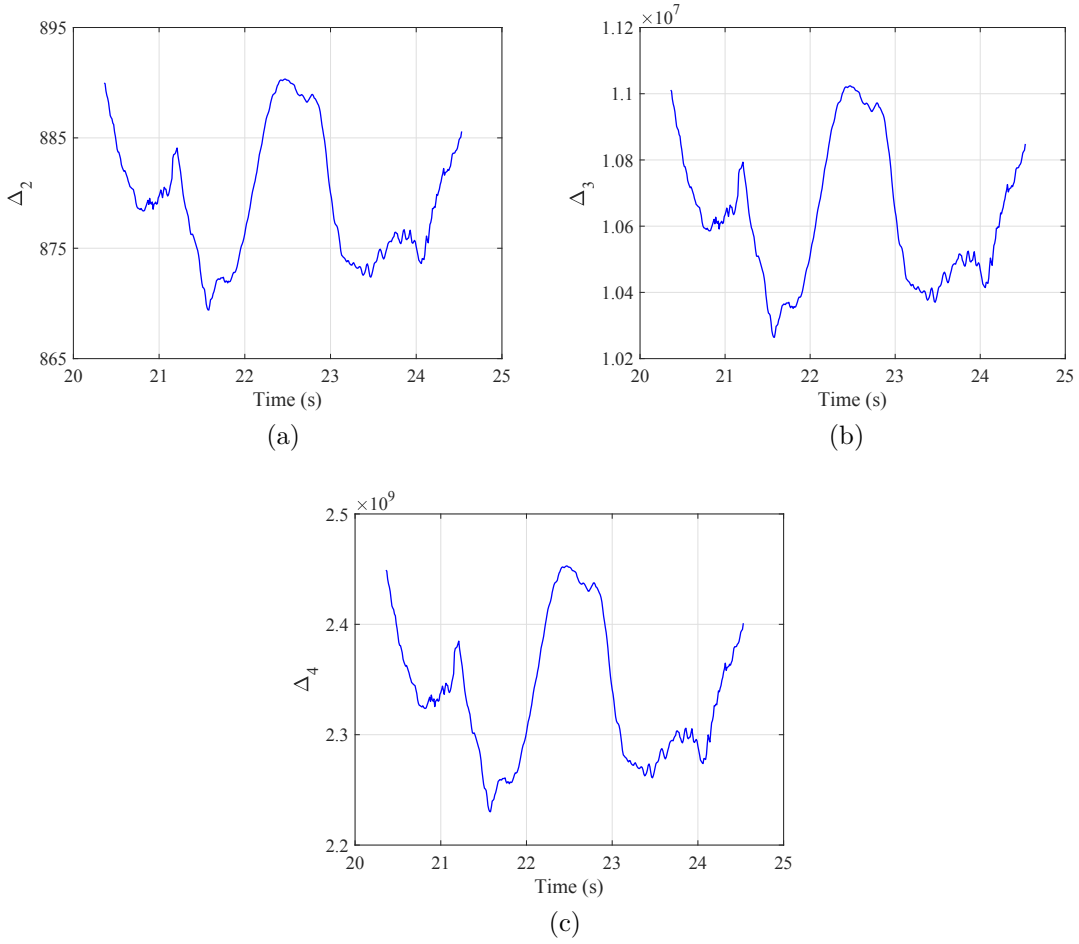

Figure 4.2: Values of the resultant matrix discriminants Δ_2 (a), Δ_3 (b), and Δ_4 (c) for an example abduction motion. All values remain greater than zero for the duration of the motion.

The joint separation from lack of closure should not be expected without traumatic motion, so only one algorithm of selecting limits θ is needed to define valid input and coupler angles for any realistic position of the humeral head. Since the θ roots near $\pm 180°$ are physiologically infeasible, the solution can be reduced to a pair of input angles that bound the protraction-retraction angle of the SC joint. One possible reason for the shoulder girdle maintaining this linkage type is the relative

consistency in its general geometry and structure among subjects. Simulations with a larger population are needed to test this hypothesis.

The second validation method for the RRSS linkage model is calculating the error between the actual solution curve in $\theta - \phi$ space and the ellipse approximation. This simplification was made to easily reduce the two linkage joint angles to a single phase angle ζ. Instead of a complicated function for the curve's radius, the ellipse axes and center can be defined with the θ roots and $\phi(\theta) = 0$. Although this simplification results in linkage angles that do not strictly satisfy kinematic closure, the impact of this can be estimated before performing the linkage angle optimization routine.

To validate this simplification, the difference in ϕ between the complete formulation (Equation 3.6) and the ellipse approximation (Equations 3.7 and 3.8) was calculated over an equal number of θ values during a motion. Example mesh plots for both functions of ϕ are shown in Figure 4.3. The error in ϕ varies over time, as the shape of Equation 3.6 changes with the position of the GH joint. The magnitude of these errors are largest near the limits of θ and are minimal near the center ($\theta = 0°$). If the predicted values of ζ are located towards the middle of the ellipse (i.e., away from multiples of 180°), then any errors in the model outputs are likely due to other factors. While testing the performance of the optimization section, the values of ζ returned by the model resided between 50° and 150° for all subjects and motions. This appears to be sufficiently far from the lateral edges of the ellipse, so the ellipse approximation should not be a major source of model inaccuracy.

In order to compare across motions, the mean absolute error (MAE) was taken over both θ and time. This was used instead of root mean square error (RMSE) so that errors could be adequately compared across motions with different durations, as

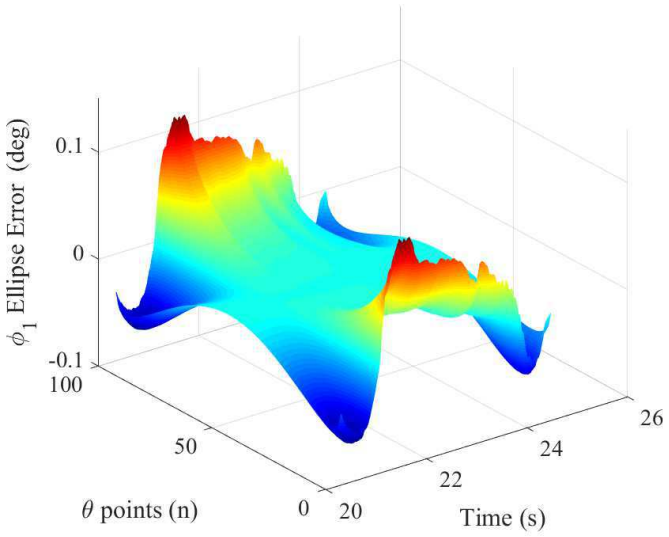

(a)

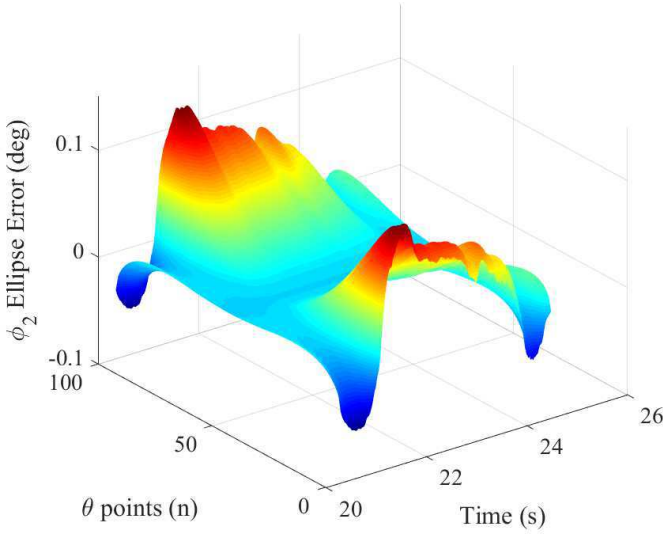

(b)

Figure 4.3: Error in coupler angle ϕ from the ellipse approximation. (a) ϕ_1 contains the error for the ellipse half below the center ($\phi < \phi_0$). (b) ϕ_2 contains the error for the ellipse half above the center. θ points near 0 and 100 are located at the lateral edges of the θ-ϕ ellipse.

RMSE tends to increase with the number of measurements [13]. The largest values for the ellipse's MAE tended to originate from a particular subject (subject 5) rather than a particular movement pattern; this suggests that skeletal geometry could impact the accuracy of this approximation. Although the maximum errors at the lateral edges of the ellipse reached errors 1° in ϕ, the MAE for all motions remained below 0.12°, which should have a minimal impact on predictions for clavicular elevation. While this is not a rigorous evaluation, the ellipse approximation would not be expected to cause large changes in the estimated shoulder girdle angles.

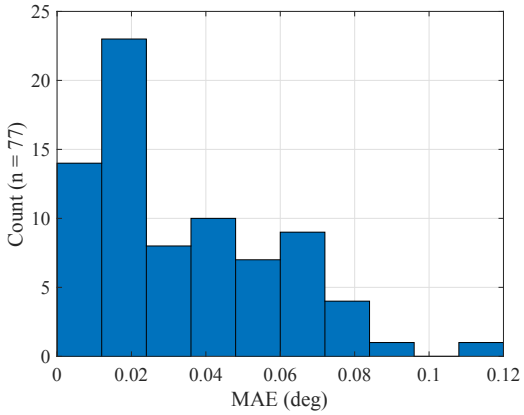

Figure 4.4: Histogram of mean absolute error from the ellipse approximation across all motions.

4.1.2 Reproduction of Measured SC and ST Angles

With the spatial linkage elements of the model validated, the next stage of model assessment focuses on the optimization routine. Since the position of the humeral head is defined at each time step, the two linkage angles ζ and η fully define the configuration of the shoulder girdle. By minimizing Equation 3.14, the angles produced by the kinematic model should match the specified STG distances for the

TS and AI landmarks. These distances are not easily measurable during dynamic motion, so this testing uses forward kinematics to estimate their location and provide ideal inputs for the optimization.

The linkage angle solutions returned by the model should satisfy two conditions. First, they should closely follow the measured data used to generate the STG distances. This can be evaluated by using from the skeletal landmark positions from the resulting ζ and η to calculate the predicted SC and ST joint angles. With ideal inputs for humeral position and STG distances, the optimization was able to successfully minimize the distance errors at the ST joint. An example of the errors is shown in Figure 4.5. For the motion shown, the optimization was able to find valid roots at all time steps and reduced the errors in STG distances to below 10 μm. The largest errors occur as the two linkage solutions approach each other and the switching routine jumps between estimates. Other increases in error may be due to the RRSS ellipse approximation or early termination of the optimization. This minimization was successfully achieved for all subjects and motions, with the largest RMSE in any motion being 0.011 mm and 0.029 mm for TS and AI, respectively.

Second, the solution selection method should properly switch between the two possible shoulder configurations. To implement this transition with minimal error, each subject needed individual-specific thresholds to control when solution transitions were allowed to occur (δ_i in Figure 3.5). These thresholds ranged from 1° to 6.5° for the five subjects studied here. Without this threshold, small oscillations or measurement errors could be treated as local minima, leading to incorrect solution switching and large jumps in shoulder angles. So, the factors that govern this threshold are dependent on anthropometry and other subject-specific criteria.

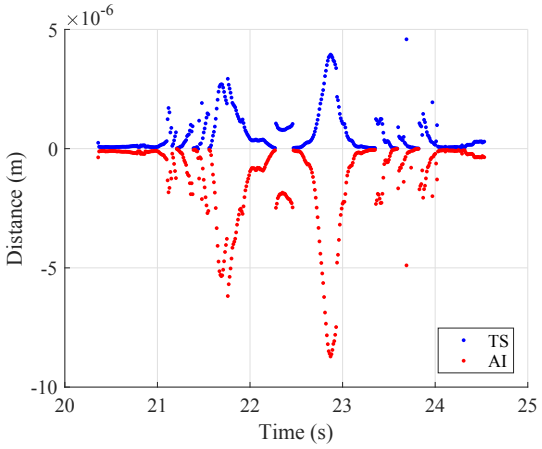

Figure 4.5: Errors in scapulothoracic gliding distances for an example abduction motion.

Example results from the model are shown in Figures 4.6 and 4.7. In each of these, the solution begins at the solution with the smaller linkage angles (dashed line). This solution selection is maintained until the distance between scapular upward rotation angles (Figure 4.6a, middle) is smaller than the specified threshold. Recognizing that minimum distance has occurred in a filtered variable introduces some delay, which accounts for some of the deviation between the solution and the measured data (Figures 4.6b and 4.7b). It then follows the solution with larger linkage angles (dash-dotted line) until another switching point is recognized. This process continues until the end of the measured data. In this example motion, the model was able to replicate the measured data very well, with only small issues around the switching points. The magnitude of these errors depended on the value of the subject's switching threshold—larger thresholds would cause larger jumps in shoulder girdle angles, while smaller thresholds could prevent solution switching from occurring.

Ideally, the two minima should merge into a single solution, allowing for a smooth transition between linkage angles. Otherwise, the shoulder girdle would have

to toggle positions in an instant, which is not physically realistic. The distance between solutions appears to be too large to be ascribed to numerical limits of the optimization method. One possible reason for this is the ellipse approximation for the RRSS input and coupler angles. This method was assumed to be sufficiently accurate based on small errors in the coupler angle ϕ. However, given the relative lengths of the clavicle and scapula, a small angular error at the SC joint could lead to larger errors in scapular orientation. The ST angles generally displayed larger jumps between solutions than the SC angles, which also supports this conjecture.

In addition, the switching algorithm did not work properly in some cases. For example, one of the most problematic movements for the model was combing hair. For all subjects, the shoulder girdle oscillated about the minimum distance point and the motion of arm elevation changed frequently. This causes the switching algorithm to switch between optimization minima at inappropriate instances. Figure 4.8 shows the chosen solution diverge from the measured angles used to generate the model inputs. Tightening the switching threshold would reject most of these incorrect toggle points, but would remove the desired switching behaviors in other motions. Using the complete equations for RRSS closure instead of the ellipse approximation may alleviate this issue as well. This would allow the threshold to be reduced enough to handle numerical optimization errors but reject false switching from these oscillations. This may also diminish the subject-specific nature of the switching threshold, as the complete RRSS linkage constraint (Equation 3.6) includes the skeletal geometry directly.

In order to assess the overall quality of the model, RMSE metrics were calculated over the duration of each motion. Each shoulder girdle angle was analyzed

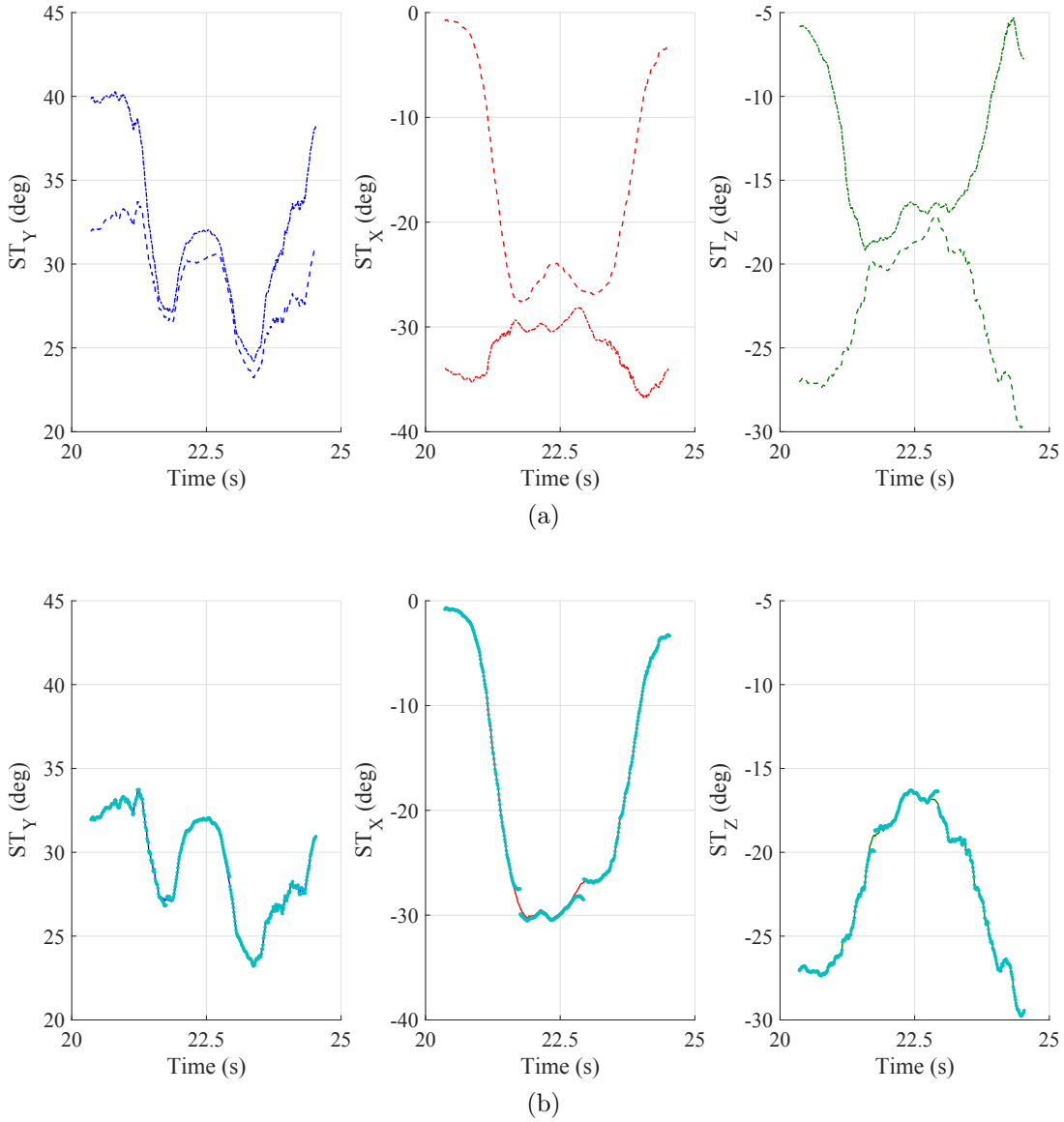

Figure 4.6: Scapulothoracic angles for an example abduction motion. (a) Comparison of the two shoulder linkage angle solutions. The dashed line is the solution with smaller linkage angles ζ and η, while the dash-dotted line is the solution with the larger linkage angles. (b) Comparison of the measured scapulothoracic angles (solid line) with the chosen solution (cyan dots).

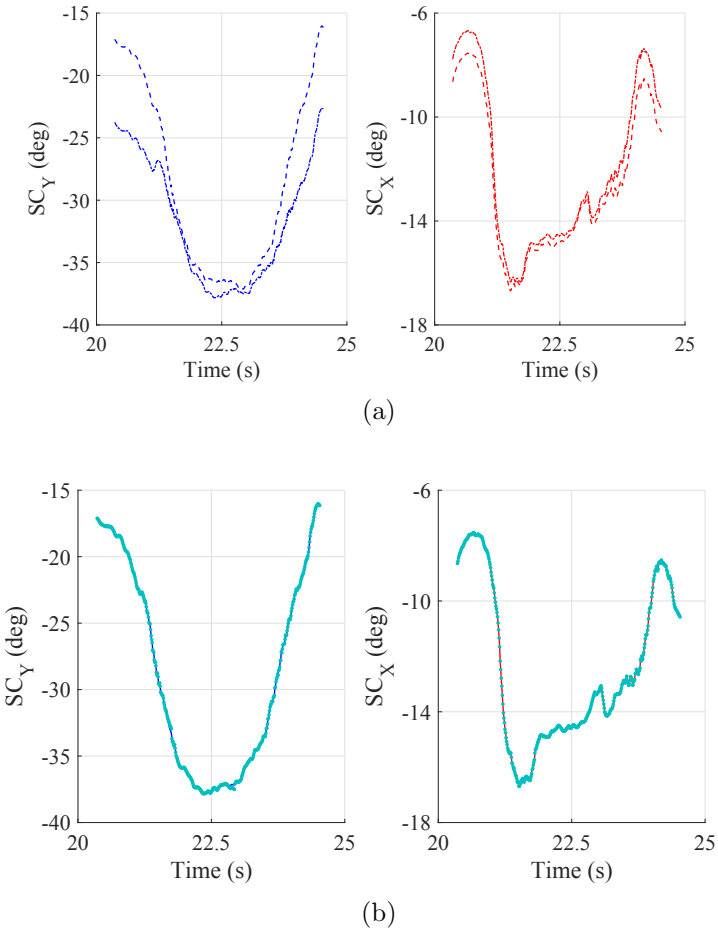

Figure 4.7: Sternoclavicular angles for an example abduction motion. (a) Comparison of the two shoulder linkage angle solutions. The dashed line is the solution with smaller linkage angles ζ and η, while the dash-dotted line is the solution with the larger linkage angles. (b) Comparison of the measured sternoclavicular angles (solid line) with the chosen solution (cyan dots).

separately for this statistical analysis. Since the range of motion differs for each angle, they cannot be meaningfully compared to determine which angles is the "least accurate". However, because the same movements are used in all parts of the validation, the statistics for these error distributions can be compared with each other across conditions. To compare the baseline performance with other simulations, the

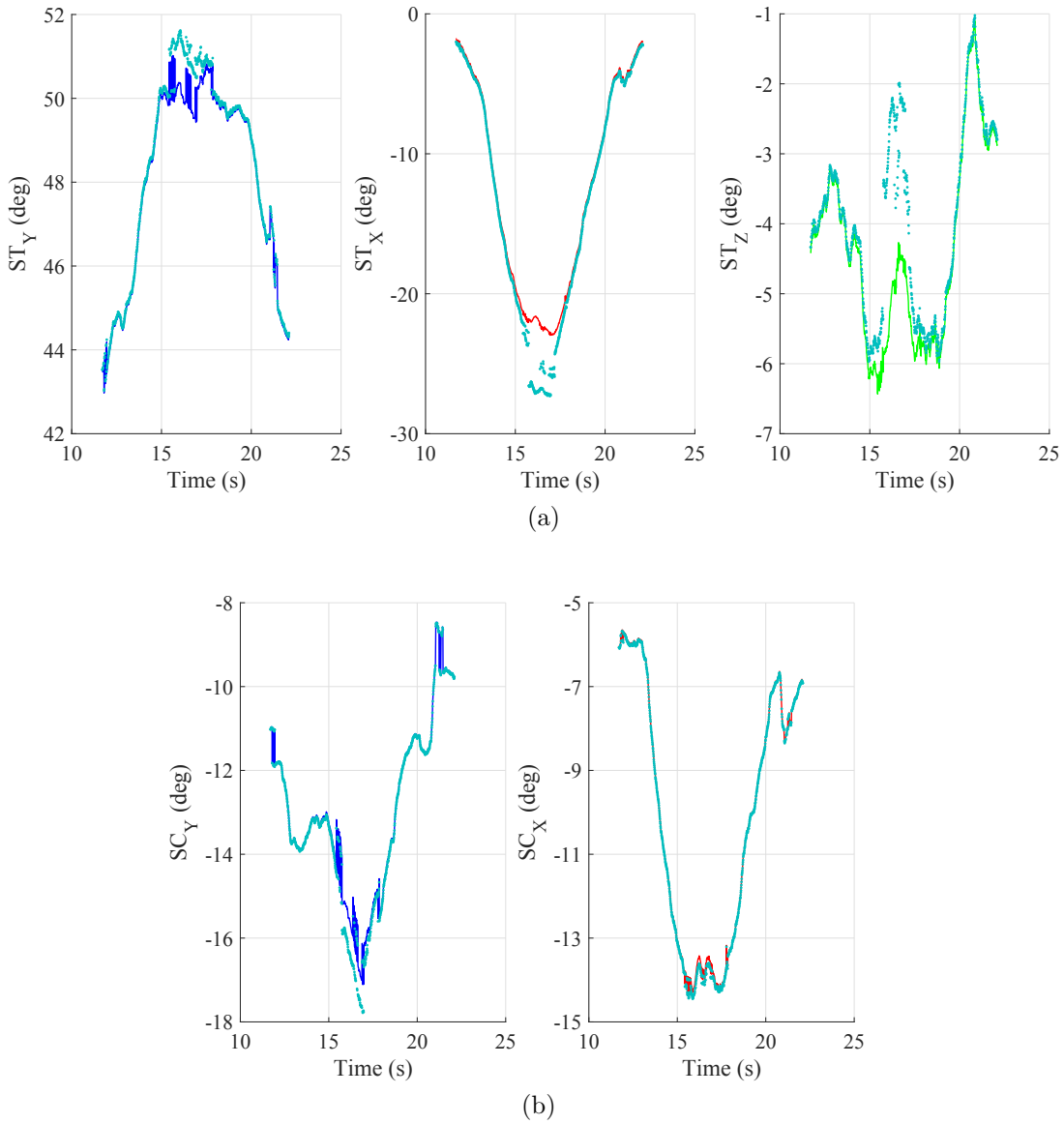

Figure 4.8: Scapulothoracic (a) and sternoclavicular (b) angles for an example combing motion. The observed points (cyan dots) fail to track the measured solution (solid line) when the switching distance remains near the subject-specific threshold.

50th and 95th percentiles with 95% confidence bounds were calculated by bootstrap resampling over 10000 iterations. These quantities for the ideal model conditions are presented in Table B.1. Overall, the kinematic model produced expected RMSE of

2° or less. The SC angle errors were substantially smaller than the ST angles, and all errors would be unlikely to cause clinical misinterpretation [71]. Thus, with ideal inputs to the model, the spatial linkage equations are able to accurately estimate the configuration of the shoulder girdle.

4.2 Sensitivity Analyses

The previous analysis showed that the proposed kinematic model is able to properly estimate the SC and ST angles of the shoulder girdle. However, these tests assumed that the kinematic information for the torso, humerus, and scapular landmarks was ideal. Using forward kinematics to estimate some of these quantities allows for systematic errors in the model to be identified, but it does not represent how the model would behave with measured data. Actual experimental data for all inputs would contain measurement noise and soft tissue artifacts that would obscure the true motion of the segments. In addition, inaccurate measurement of anthropometric quantities cause the model to solve for shoulder angles according to this different geometry. Both of these error sources could lead to data that does not conform to the ideal joint models and introduce errors into the shoulder angle predictions. This sensitivity analysis covers length offsets in the shoulder skeleton as well as additive noise in the model inputs to determine how robust the model is to these error sources. Since forward kinematics is used to formulate ideal estimates of humerothoracic motion and STG distances, these changes are applied between those calculations and the RRSS linkage model to create internal discrepancies among the inputs, anthropometry, and constraints.

4.2.1 Clavicle Length

The length of the clavicle is defined as the distance between the SC and AC joints. This distance may not be measured accurately because the lateral endpoint is difficult to palpate and does not match the AC skeletal landmark. In addition, the behavior of the SC and AC joints is often modeled as simple spherical joints, which may not be sufficiently accurate. The anatomy of these joints varies significantly between subjects and can be categorized into one of several variants by the geometry and arrangement of articular structures [29, 30].

The magnitude of errors for this length was based on the estimated measurement accuracy of a single point and the number of points required for this. Although the marker accuracy for this data was not explicitly given, it was assumed that the system from an earlier study was used to collect this data, which stated an accuracy of 0.3 mm [92]. This was added to an estimated 1 mm error from the palpation and marker placement to find the maximum error for a single position. To convert this position error to a segment geometry error, this quantity is multiplied by the square root of the number of points needed for this estimation (in this case, two—the SC and AC joint centers). This method gives a maximum error in clavicle length around 1.8 mm. The model was simulated for all motions with this value added to and subtracted from the nominal length.

The RMSE metrics for these simulations are contained in Tables B.2 and B.3. These errors are substantially larger than those measured under ideal conditions, with most RMSE percentiles being about an order of magnitude larger than baseline. For example, half of the RMSE in scapular upward rotation (ST_X) with a shorter clavicle is expected to exceed 8.89°, which is above the proposed threshold for differences in

clinical interpretation [71]. Example scapulothoracic angles for this case are shown in Figure 4.9. The errors for the lengthened clavicle are even more severe, with errors in upward rotation surpassing 30°. These large errors may be related to the relative lengths of the clavicle and scapula in the serial shoulder skeleton. Since the clavicle is significantly longer than the distance between the AC and GH joints, changing the length of the clavicle would require substantial adjustment of the scapula about the GH joint, increasing the error in ST angles. Some errors would also be present in the SC angles, as the linkage must maintain kinematic closure and match the original STG distances.

One interesting observation from this part of the analysis is the difference in optimization solution behavior. For smaller clavicle lengths, the pair of optimization minima merged into a single point for a substantial duration of most movements (Figure 4.9a). In contrast, extending the length of the clavicle increased the distance between the roots such that they never crossed during the motions. This provides insight into the issues with the current switching method by showing its strong dependence on anthropometry. Small changes in joint centers or the RRSS ellipse approximation, thought to be insignificant during the design process, could have introduced the need for subject-specific switching thresholds. This improvement can be pursued in the near future.

4.2.2 Distance from Acromioclavicular Joint to Glenohumeral Joint

The distance between the AC and GH joints is another likely source of error because it cannot be measured non-invasively. Instead, a three-dimensional scaling matrix was used to estimate the GH joint center from cadaver data and other scapular landmarks [7, 60], This method assumes proportional changes to all aspects of the

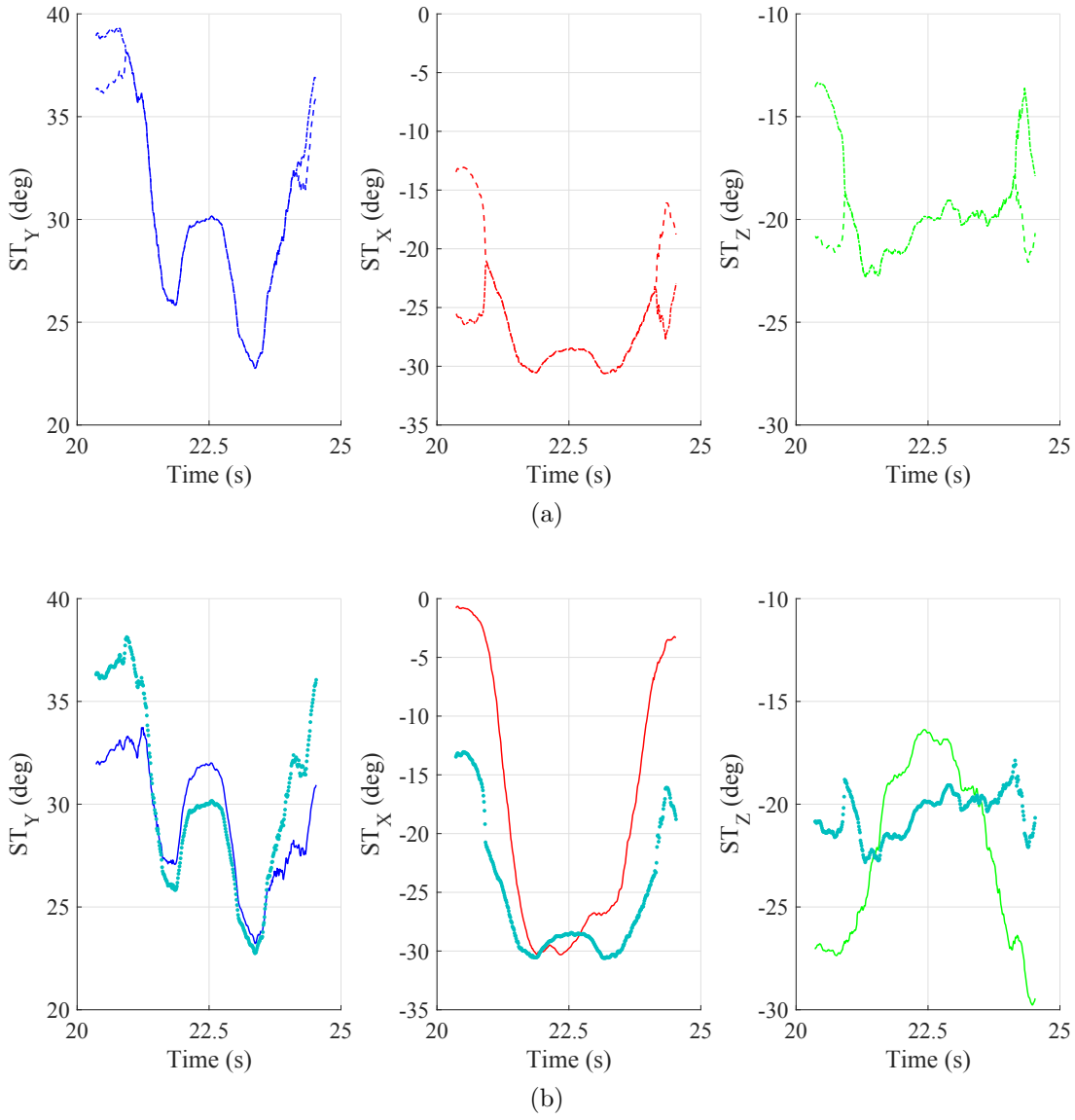

Figure 4.9: Scapulothoracic angles for an example abduction motion with shortened clavicle. (a) Comparison of the two shoulder linkage angle solutions. The dashed line is the solution with smaller linkage angles ζ and η, while the dash-dotted line is the solution with the larger linkage angles. (b) Comparison of the measured scapulothoracic angles (solid line) with the chosen solution (cyan dots).

bone, which cannot be validated without invasive measurements from the subjects. Since the landmarks used for this method (AA, TS, AI) were on the posterior side

of the scapula, structures on the anterior side of the scapula, such as the glenoid and coracoid, are not guaranteed to scale identically. So, this method could have introduced error into the geometry of the shoulder linkage. Although several points are needed for this calculation to both define and apply this transformation, only the three landmarks used in the scaling were considered for choosing the maximum error of 2.25 mm.

The results of these geometry changes are contained in Tables B.4 and B.5. The RMSE distributions are similar to those from the clavicle length analysis and highlight similar issues. By forcing the model to strictly follow kinematic closure, small errors in shoulder girdle dimensions result in substantial estimate changes. Since this distance cannot be measured precisely in most situations, these errors should be expected when applying this model to other experiments. Also, since the humeral head translates up to 5 mm relative to the glenoid during normal motion [43,65], this error will likely occur during any arm movement. This hampers adoption of the model in a clinical settings, where patients with shoulder injuries may have abnormally lax joint capsules that allow for more translation of the humeral head.

4.2.3 Scapulothoracic Ellipsoid Size

The final anthropometric measure studied here is the size of the scapulothoracic gliding ellipsoid. This approximation of the ribcage is critical to the optimization process for determining the orientation of the scapula. This static geometry does not account for costal movement during breathing and rotation of the spine. For this analysis, the ellipsoid axes were changed in each coordinate direction (x, y, z) by 2.6 mm, 2.6 mm, and 1.8 mm, respectively, according to the number of points used to generate the axes. The x- and y-axes used the intrajugular notch, the C7 vertebra,

the T8 vertebrae, and the xiphoid process. The z-axis is defined with the intrajugular notch and the lateral edge of the thorax.

The results of this analysis are presented in Tables B.6 and B.7. While these changes still created larger errors than the baseline results, the increases were smaller than expected. Excluding potential outliers in scapular upward rotation and posterior tilt that inflate the 95th percentiles for the smaller ellipsoid, the model appears to be less sensitive to the size of the ribcage than to the anthropometry of the clavicle and scapula. One possible reason for this is the arrangement of the shoulder's internal DOF permits simpler adjustments to these changes. Expansion or contraction of the thorax moves the medial border of the scapula in a way that resembles scapular winging. This winging could be accounted for by small changes in the linkage angle η instead of the more drastic corrections taken for other geometry changes.

4.2.4 Humeral Head Position

The position of humeral head is a certain source of error in the linkage model. This feature is not easily palpable and shows significant motion during normal arm movements. Non-invasive estimates, such as those from the Instantaneous Helical Axis method, are commonly used to estimate the GH joint center. However, these methods provide significantly different results from medical imaging techniques, with errors in center estimates around 1.5 cm or greater [92]. To be implemented in other settings, the linkage model should be able to withstand this type of error. The measurement error for this point was defined as normally distributed noise in each Cartesian direction with a specified standard deviation.

The results of this test are presented in Table B.8. Ultimately, a standard deviation of 0.25 mm was used for this analysis. This unrealistically low value was necessary to prevent the model from failing to find a feasible solution for some motions. Still, even with such a small amount of error, the RMSE errors for the ST angles are worse than any of the aforementioned geometry changes. One interesting feature of the RMSE metrics is that SC joint angles were not affected much by this noise, while the ST joint angles show the worst performance compared to the other tests. Furthermore, scapular protraction (ST_X) a large proportion of errors above 40° and even some around 90°. This should not be possible with as a valid scapular configuration, which suggests that even this level of noise prevented valid configurations from some motions. Regardless, the model failed to estimate scapular angles for even a small amount of added noise. This level of noise is much lower than any reasonable expectation for humeral head motion. When combined with the model's sensitivity to the distance between the AC and GH joints, ignoring the translation of the humeral head is an inappropriate simplification of shoulder motion. A model that assumes ideal joint rotations at the GH joint should not be used in isolation for estimating shoulder angles. Instead, this kinematic constraint could be paired with a compliant GH joint or other modeling elements for a trade-off between ideal joint behavior and noise tolerance.

4.2.5 Scapulothoracic Gliding Constraints

The final part of the sensitivity analysis addresses measurement noise in the STG distances. These distances lack a standardized measurement method, but they still serve as a key input to the optimization routine. These distances are used as the two inputs needed to fully define the remaining two DOF of the shoulder girdle. For

the immediate future, this value would need to be estimated from palpation during static postures or from a regression model. To test the impact of potential errors on the behavior of the model, small perturbations were added to each of these distances individually. Normally distributed noise was added to the forward kinematics estimates with a standard deviation of 1 mm.

The RMSE metrics for these tests are contained in Tables B.9 and B.10. Similar to humeral head position, using errors with a wider distribution resulted in optimization failure for some motions. The magnitudes of the errors are also comparable between these cases. It is possible that random noise in any of the kinematic inputs would produce this level of shoulder angle error. Even though the measured data could be filtered before using this model, it is unlikely that the noise would be sufficiently suppressed to allow for correct angle estimation. So, the linkage model should not be used in its current state for predicting shoulder angles from kinematic data.

One final observation from the sensitivity analysis is that the errors for this test are much larger than those from the dilation of the scapulothoracic ellipsoid. The current test produced some of the largest ST angle errors, while the ellipsoid size change produces some of the best errors overall. This may be due to how the parameters were changed in each case. Changing the size of the ellipsoid moves both TS and AI smoothly, while adding random noise to only one landmark distance can introduce errors about all axes of the scapular reference frame. However, the large scapular protraction errors show that these tests experience the same issue as the humeral head test and is producing scapular angles that should not be reached. So, the effects of applying noise to only one landmark are probably overshadowed by the model's sensitivity to any random noise.

4.3 Comparison with Existing Regression Models

The performance of the kinematic model should also be compared with existing regression models. Although the model performed poorly when subject to imperfect inputs, the kinematic closure principle should still outperform the regression models under ideal conditions. Since the regression models minimize error across the predictors used in the design process, they are unable to achieve perfect tracking of the shoulder girdle angles for any subject. If the performance of the linkage model is comparable to that of the regression models, then it is difficult to justify the added complexity of the spatial linkage method.

Two regression equations were used in this comparison. The first model was developed by de Groot and Brand [19] and is referred to hereafter as the Dutch shoulder rhythm (DSR). This model was chosen due to its prominence among shoulder motion regression methods. For example, it has been used in one of the most prominent upper limb musculoskeletal models for its shoulder girdle motion [19]. This model was designed with measured joint angles during loaded, closed-chain poses of the arm. The linear regression model estimates SC and ST angles from HT plane of elevation, HT elevation angle, the direction of force application, and the initial joint angles at rest. Since the data used to evaluate the model consists of open-chain movements, the force direction was set to zero [123]. The initial joint angles were estimated from landmark positions collected while the subjects were at rest.

The second model was recently developed by Xu et al. and is also known as the Liberty Mutual shoulder rhythm (LMSR). This model was developed from a wider array of static posture without loading the arm and was chosen for its improved accuracy relative to other shoulder regressions [123]. The version of the regression tested

here uses linear, quadratic, and two-term interactions of humerothoracic angles to predict clavicular and scapular angles. Although the testing conditions and measurement tools used for these models are not the same as those used in the measured data, assessing these models will allow for the impact of subject and task generalization to be determined.

The RMSE metrics for these regression equations are shown in Tables B.11 and B.12. Figure 4.10 shows that all models produce the same trends in joint angles during a motion. But, both regression models had significantly larger errors than the ideal model, with median RMSE in excess of 6° for all shoulder angles. The regression models also resulted in joint angles that may not be feasible for certain motions. For example, the clavicle orientation predicted by the DSR and LMSR models is retracted and elevated to a much greater degree than the measured data would suggest. Although there are substantial differences between estimates for posterior tilt of the scapula (Figure 4.10c), this is likely due to measurement errors in the original dataset. Near the start of some motion, shoulder angles were also measured with a palpating fixture on the scapular landmarks. These supplemental measurements revealed that the acromial marker cluster tends to report greater anterior tilt than should be expected for these movements.

Also, the comparison between the two regression models is generally in agreement with the findings of Xu et al. [123]. In that comparison, the DSR model performed worse than the LMSR model for every shoulder angle. This conclusion holds in this testing for all angles except clavicular elevation (SC_X). This may be due to the inclusion of dynamic motions that reached across the sagittal plane or behind the back, neither of which were included in the design or testing of the regression models.

Another possibility is that clavicular elevation for dynamic motion is more similar in loaded static postures than in unloaded ones. Recruitment of similar shoulder girdle muscles may be occurring in both the dynamic and loaded situations, leading to reduced errors in the DSR.

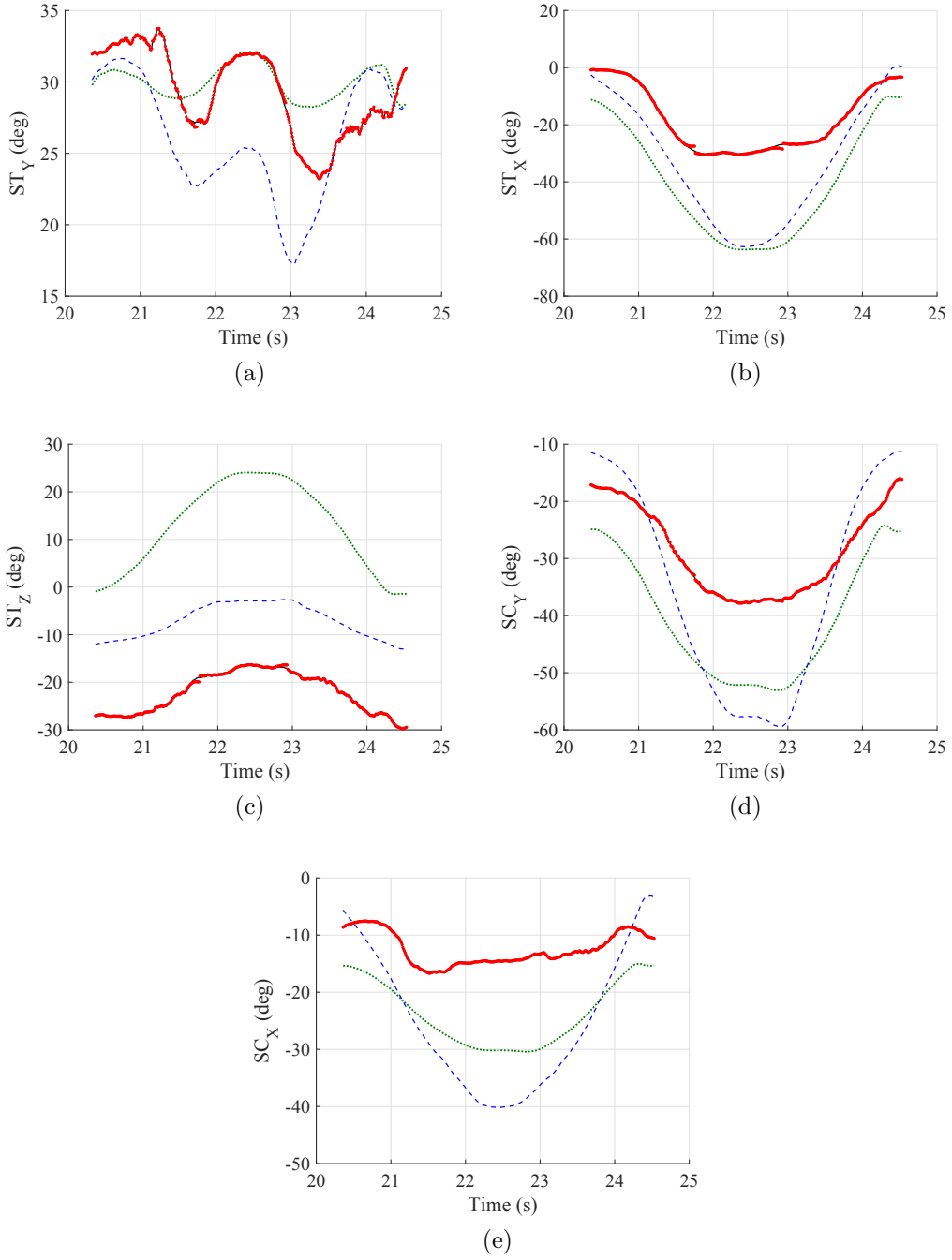

Figure 4.10: Shoulder angle estimates from existing regression models and linkage model for an example abduction motion. Red dots: Shoulder linkage model. Green dotted line: de Groot and Brand model (DSR). Blue dashed line: Xu et al. model (LMSR). Black solid line: measured data, mostly covered by linkage model.

Chapter 5

Conclusion

This thesis describes a kinematic shoulder model for estimating the joint angles of the shoulder girdle without any sensing elements on the clavicle or scapula. This is accomplished by applying kinematic constraint equations from a RRSS spatial linkage to the motion of the humerus, torso, and medial border of the scapula. By removing the need for acromial sensing or other traditional measurement methods at the shoulder girdle, the model should be able to estimate the full shoulder configuration in environments that prohibit these techniques, such as robotic exoskeletons and spacesuits.

With ideal humerothoracic measurement and STG distance values, the model was able to estimate the configuration of the shoulder girdle with reasonable accuracy. Root mean square errors were expected to be less than 2°, which is sufficiently accurate for clinical assessment and decision making. In addition, the linkage model followed similar motion trends as existing shoulder models, but did so with significantly less error. So, in the best case scenario, the model is able to predict clavicular and scapular angles without sensing elements on the acromion and is more capable than existing estimation methods.

However, when the skeletal geometry or inputs deviate from ideal conditions, the errors in predicted shoulder angles increase significantly. Kinematic closure was used as the primary means to determine shoulder configuration without measured SC

and ST angles. But, this became a limitation when segment geometry or position data was altered. Changes in clavicular or scapular dimensions resulted in substantial errors and incorrect root switching behavior. Adding small amounts of noise to the input humerothoracic kinematics and STG distances caused the model to produce even larger errors and infeasible scapular configurations. So, although the regression models are limited on how well they can describe the motion of a single subject, they are the more appropriate option for studying shoulder motion in an experimental setting.

Despite these issues, there are two immediate ways the shoulder linkage model can be enhanced. First, the solution selection performance under ideal conditions can be improved to smoothly transition between optimization minima. During most arm motions in the experimental dataset, the optimization solutions fail to converge to a single pair of linkage angles, resulting in discontinuities when the accepted solution is changed. One likely cause for this is the approximation of the RRSS kinematic constraints as an ellipse. Although the error in the RRSS mechanism coupler angle is small within the expected range of SC angles, this restricts the optimization method to use angles that do not truly satisfy kinematic closure. The baseline analysis should be repeated with the full equation for the coupler angle (Equation 3.6) to confirm this. If this change is insufficient, then interpolation or filtering methods could be added to the switching routine for improved prediction around the toggle points. While this fallback does not have a clear theoretical justification, it should still reduce the shoulder angles errors when changing minima.

Second, the dependence on STG distances as optimization inputs impedes the model's use in biomechanics studies. As mentioned in Section 1.4, the acromion has

become the standard location for measuring the movement of the scapula because of reduced soft tissue artifacts. There has been a continual lack of developed methods for measuring scapular winging distances during dynamic movements. Requiring these distances to perform the shoulder linkage optimization limits the applicability to experiments with static arm postures. One alternative is to utilize a mixed effects model or other regression techniques to predict these distances from anthropometry and humerothoracic motion. This resembles the shoulder regression models currently used in research, but the predicted distances would be used for kinematic constraints at the ST joint. However, this method may not be directly compatible with the closure constraint, as the model outcomes would not be able to consistently produce scapulothoracic distances that matched the both orientation of the scapula and the position of the GH joint center.

Nevertheless, this work still provides an important contribution to the field of shoulder biomechanics. This thesis describes the first model of the shoulder that uses kinematic constraints and humerothoracic motion to estimate the angles of the clavicle and scapula. Under ideal conditions, it was able to significantly outperform two existing regression models. It also showed that exact kinematic closure may be too strict of a condition to use by itself for modeling the shoulder complex. Instead, the spatial mechanism principles could be integrated into a more detailed shoulder model with compliant joints or a force-based optimization scheme. If incorporated successfully, the spatial linkage model would allow for the prediction of shoulder girdle motion during complex interaction tasks. This would benefit both robotic exoskeletons and spacesuits by improving the shoulder motion estimates needed for functional assessment, control strategies, and hardware evaluation while remaining robust to measurement inaccuracies.

Appendices

Appendix A

Permission for Use of Human Subject Data

The following license was distributed with the anonymized human subject data used in this work. The data can be found on the OpenSim project page for the Delft Shoulder and Elbow Model (https://simtk.org/projects/dsem).

Appendix B

Tables of Root Mean Square Errors

These tables contain root mean square error (RMSE) metrics for estimated shoulder joint angles (see Chapter 4). SC_Y and SC_X represent clavicular protraction-retraction and depression-elevation, respectively. ST_Y, ST_X, and ST_Z represent scapulothoracic protraction-retraction, downward-upward rotation, and posterior-anterior tilt, respectively. 50th and 95th percentiles of the sample data along with 95% confidence intervals for shown for each test. These values were calculated through bootstrapping in MATLAB over 10000 resample iterations. "LB" stands for lower bound of the confidence interval, and "UB" stands for the upper bound. All RMSE sample groups were confirmed to come from significantly different distributions than the baseline data with the Wilcoxon signed-rank test.

Table B.1: Estimates and 95% percent confidence intervals for the RMSE percentiles of shoulder girdle angles: RRSS model and ideal inputs.

	SC_Y	SC_X	ST_Y	ST_X	ST_Z
50th, LB	0.04	0.02	0.05	0.23	0.11
50th Percentile	0.05	0.03	0.06	0.29	0.16
50th, UB	0.08	0.03	0.09	0.45	0.25
95th, LB	0.22	0.12	0.43	1.17	0.72
95th Percentile	0.27	0.14	0.58	1.51	0.86
95th, UB	0.41	0.19	0.73	2.19	1.68

Table B.2: Estimates and 95% percent confidence intervals for the RMSE percentiles of shoulder girdle angles: RRSS model with reduced clavicle length by 1.8 mm.

	SC_Y	SC_X	ST_Y	ST_X	ST_Z
50th, LB	1.40	0.31	2.16	7.73	3.79
50th Percentile	1.53	0.49	2.28	8.89	4.25
50th, UB	1.67	0.70	2.46	9.51	4.52
95th, LB	1.99	1.08	3.40	13.84	8.73
95th Percentile	2.21	1.13	4.08	15.37	8.98
95th, UB	3.06	1.24	4.72	16.79	9.61

Table B.3: Estimates and 95% percent confidence intervals for the RMSE percentiles of shoulder girdle angles: RRSS model with increased clavicle length by 1.8 mm.

	SC_Y	SC_X	ST_Y	ST_X	ST_Z
50th, LB	1.87	0.58	4.37	12.74	4.58
50th Percentile	2.08	0.73	4.83	13.30	5.32
50th, UB	2.29	1.06	5.25	14.31	6.66
95th, LB	7.21	1.43	9.93	34.55	30.94
95th Percentile	8.47	1.52	13.67	37.77	35.21
95th, UB	10.91	1.64	23.70	45.41	43.67

Table B.4: Estimates and 95% percent confidence intervals for the RMSE percentiles of shoulder girdle angles: RRSS model with reduced length between AC and GH joints by 2.25 mm.

	SC_Y	SC_X	ST_Y	ST_X	ST_Z
50th, LB	1.14	0.68	2.48	9.14	2.83
50th Percentile	1.52	0.82	2.71	9.86	3.28
50th, UB	1.80	1.05	3.09	10.67	3.81
95th, LB	6.35	1.42	6.14	31.96	28.09
95th Percentile	7.67	1.51	9.58	35.31	32.52
95th, UB	10.49	1.60	21.32	44.22	40.85

Table B.5: Estimates and 95% percent confidence intervals for the RMSE percentiles of shoulder girdle angles: RRSS model with increased length between AC and GH joints by 2.25 mm.

	SC_Y	SC_X	ST_Y	ST_X	ST_Z
50th, LB	0.85	0.73	1.12	4.42	2.10
50th Percentile	1.07	0.82	1.29	5.53	2.93
50th, UB	1.21	1.05	1.49	6.78	3.40
95th, LB	1.61	1.35	2.25	11.36	5.32
95th Percentile	1.88	1.39	3.00	13.03	5.94
95th, UB	5.10	1.44	4.34	25.40	18.57

Table B.6: Estimates and 95% percent confidence intervals for the RMSE percentiles of shoulder girdle angles: RRSS model with reduced scapulothoracic ellipsoid axes.

	SC_Y	SC_X	ST_Y	ST_X	ST_Z
50th, LB	0.27	0.12	1.16	1.60	0.58
50th Percentile	0.39	0.16	1.46	2.37	0.90
50th, UB	0.50	0.18	1.82	3.08	1.35
95th, LB	4.76	1.73	4.00	24.16	24.49
95th Percentile	5.96	2.02	5.73	26.69	27.41
95th, UB	7.27	2.38	9.66	29.11	34.75

Table B.7: Estimates and 95% percent confidence intervals for the RMSE percentiles of shoulder girdle angles: RRSS model with increased scapulothoracic ellipsoid axes.

	SC_Y	SC_X	ST_Y	ST_X	ST_Z
50th, LB	0.16	0.03	1.08	0.64	0.47
50th Percentile	0.18	0.04	1.20	0.76	0.55
50th, UB	0.22	0.05	1.34	0.92	0.63
95th, LB	0.37	0.15	2.13	2.03	1.03
95th Percentile	0.50	0.17	2.17	2.98	1.29
95th, UB	1.46	0.22	2.66	7.46	3.31

Table B.8: Estimates and 95% percent confidence intervals for the RMSE percentiles of shoulder girdle angles: RRSS model with up to 0.75 mm of noise added to the position of the humeral head.

	SC_Y	SC_X	ST_Y	ST_X	ST_Z
50th, LB	0.62	0.23	42.45	8.70	10.65
50th Percentile	0.81	0.27	45.22	10.03	11.54
50th, UB	1.47	0.31	50.35	13.22	13.37
95th, LB	2.48	0.62	85.15	30.12	51.39
95th Percentile	3.24	0.69	91.29	34.62	56.78
95th, UB	5.45	1.24	98.80	44.70	64.64

Table B.9: Estimates and 95% percent confidence intervals for the RMSE percentiles of shoulder girdle angles: RRSS model with up to 3 mm of noise added to the distance between TS and the ribcage.

	SC_Y	SC_X	ST_Y	ST_X	ST_Z
50th, LB	0.61	0.17	41.69	8.56	10.65
50th Percentile	0.87	0.24	44.93	9.73	11.64
50th, UB	1.38	0.33	50.38	13.44	13.59
95th, LB	2.28	0.58	85.15	28.22	51.43
95th Percentile	3.19	0.68	91.21	33.81	56.75
95th, UB	5.45	1.23	98.51	44.65	64.57

Table B.10: Estimates and 95% percent confidence intervals for the RMSE percentiles of shoulder girdle angles: RRSS model with up to 3 mm of noise added to the distance between AI and the ribcage.

	SC_Y	SC_X	ST_Y	ST_X	ST_Z
50th, LB	0.65	0.18	41.51	8.83	10.70
50th Percentile	0.85	0.24	45.48	10.16	11.82
50th, UB	1.36	0.33	50.20	13.73	14.09
95th, LB	2.75	0.60	85.07	30.80	51.44
95th Percentile	3.28	0.70	91.39	35.41	56.85
95th, UB	5.47	1.24	98.90	44.92	64.65

Table B.11: Estimates and 95% percent confidence intervals for the RMSE percentiles of shoulder girdle angles: de Groot and Brand model (DSR).

	SC_Y	SC_X	ST_Y	ST_X	ST_Z
50th, LB	14.32	5.22	7.59	9.70	7.20
50th Percentile	15.13	6.23	8.74	11.14	8.22
50th, UB	16.22	7.88	9.77	13.50	9.38
95th, LB	20.24	11.74	13.15	22.81	34.37
95th Percentile	22.14	12.66	14.29	24.18	35.46
95th, UB	25.31	14.61	19.80	28.10	39.45

Table B.12: Estimates and 95% percent confidence intervals for the RMSE percentiles of shoulder girdle angles: Xu et al. model (LMSR).

	SC_Y	SC_X	ST_Y	ST_X	ST_Z
50th, LB	6.57	9.01	5.40	6.44	6.80
50th Percentile	7.08	9.89	7.04	7.54	8.28
50th, UB	7.92	11.02	8.44	9.92	10.15
95th, LB	12.92	18.36	11.83	18.62	20.06
95th Percentile	15.12	20.09	13.07	21.18	24.53
95th, UB	19.42	23.67	16.54	22.77	28.78

Bibliography

[1] Andrew Abercromby, Scott Cupples, Sudhakar Rajulu, Jesse Buffington, Jason Norcross, and Steven Chappell. Integrated extravehicular activity (EVA) human research plan: 2016. In *46th International Conference on Environmental Systems*, 2016.

[2] A Anderson, A Hilbert, P Bertrand, S McFarland, and DJ Newman. In-suit sensor systems for characterizing human-space suit interaction. In *44th International Conference on Environmental Systems*, 2014.

[3] Allison P Anderson, Dava J Newman, and Roy E Welsch. Statistical evaluation of causal factors associated with astronaut shoulder injury in space suits. *Aerospace Medicine and Human Performance*, 86(7):606–613, 2015.

[4] Stephen D Bagg and William J Forrest. A biomechanical analysis of scapular rotation during arm abduction in the scapular plane. *American Journal of Physical Medicine & Rehabilitation*, 67(6):238–245, 1988.

[5] H Bao and PY Willems. On the kinematic modelling and the parameter estimation of the human shoulder. *Journal of Biomechanics*, 32(9):943–950, 1999.

[6] Pierre J Bertrand, Allison Anderson, Alexandra Hilbert, and Dava J Newman. Feasibility of spacesuit kinematics and human-suit interactions. In *44th International Conference on Environmental Systems*, 2014.

[7] Dimitra Blana, Juan G Hincapie, Edward K Chadwick, and Robert F Kirsch. A musculoskeletal model of the upper extremity for use in the development of neuroprosthetic systems. *Journal of biomechanics*, 41(8):1714–1721, 2008.

[8] Bart Bolsterlee, DirkJan HEJ Veeger, and Edward K Chadwick. Clinical applications of musculoskeletal modelling for the shoulder and upper limb. *Medical & Biological Engineering & Computing*, 51(9):953–963, 2013.

[9] Bart Bolsterlee, HEJ Veeger, and Frans CT van der Helm. Modelling clavicular and scapular kinematics: from measurement to simulation. *Medical & Biological Engineering & Computing*, 52(3):283–291, 2014.

[10] Elizabeth Brackbill. A novel method of scapular tracking using tissue deformation. Master's thesis, University of Delaware, 2008.

[11] DJJ Bregman, S van Drongelen, and HEJ Veeger. Is effective force application in handrim wheelchair propulsion also efficient? *Clinical Biomechanics*, 24(1):13–19, 2009.

[12] Sylvain Brochard, Mathieu Lempereur, and Olivier Rémy-Néris. Double calibration: an accurate, reliable and easy-to-use method for 3D scapular motion analysis. *Journal of Biomechanics*, 44(4):751–754, 2011.

[13] Tianfeng Chai and Roland R Draxler. Root mean square error (RMSE) or mean absolute error (MAE)?–Arguments against avoiding RMSE in the literature. *Geoscientific Model Development*, 7(3):1247–1250, 2014.

[14] Iain W Charlton and GR Johnson. A model for the prediction of the forces at the glenohumeral joint. *Proceedings of the Institution of Mechanical Engineers, Part H: Journal of Engineering in Medicine*, 220(8):801–812, 2006.

[15] Ernest A Codman. *The Shoulder. Rupture of the Supraspinatus Tendon and Other Lesions in or about the Subacromial Bursa.* 1934.

[16] Elsie Culham and Malcolm Peat. Functional anatomy of the shoulder complex. *Journal of Orthopaedic & Sports Physical Therapy*, 18(1):342–350, 1993.

[17] PR Culmer, AE Jackson, SG Makower, JA Cozens, MC Levesley, M Mon-Williams, and B Bhakta. A novel robotic system for quantifying arm kinematics and kinetics: Description and evaluation in therapist-assisted passive arm movements post-stroke. *Journal of Neuroscience Methods*, 197(2):259–269, 2011.

[18] Liesbet De Baets, Rob van der Straaten, Thomas Matheve, and Annick Timmermans. Shoulder assessment according to the international classification of functioning by means of inertial sensor technologies: a systematic review. *Gait & Posture*, 2017.

[19] JH de Groot and R Brand. A three-dimensional regression model of the shoulder rhythm. *Clinical Biomechanics*, 16(9):735–743, 2001.

[20] Jurriaan H de Groot, Edward R Valstar, and Henk J Arwert. Velocity effects on the scapulo-humeral rhythm. *Clinical Biomechanics*, 13(8):593–602, 1998.

[21] Scott L Delp, Frank C Anderson, Allison S Arnold, Peter Loan, Ayman Habib, Chand T John, Eran Guendelman, and Darryl G Thelen. OpenSim: open-

source software to create and analyze dynamic simulations of movement. *IEEE Transactions on Biomedical Engineering*, 54(11):1940–1950, 2007.

[22] WT Dempster. Mechanisms of shoulder movement. *Archives of Physical Medicine and Rehabilitation*, 46:49–70, 1965.

[23] Clark R Dickerson, Don B Chaffin, and Richard E Hughes. A mathematical musculoskeletal shoulder model for proactive ergonomic analysis. *Computer Methods in Biomechanics and Biomedical Engineering*, 10(6):389–400, 2007.

[24] Lucy E Dunne, Sarah Brady, Barry Smyth, and Dermot Diamond. Initial development and testing of a novel foam-based pressure sensor for wearable sensing. *Journal of NeuroEngineering and Rehabilitation*, 2(1):4, 2005.

[25] Sonia Duprey, Alexandre Naaim, Florent Moissenet, Mickaël Begon, and Laurence Chèze. Kinematic models of the upper limb joints for multibody kinematics optimisation: An overview. *Journal of Biomechanics*, 2016 (in press).

[26] Z Dvir and N Berme. The shoulder complex in elevation of the arm: a mechanism approach. *Journal of Biomechanics*, 11(5):219–225, 1978.

[27] D David Ebaugh, Philip W McClure, and Andrew R Karduna. Effects of shoulder muscle fatigue caused by repetitive overhead activities on scapulothoracic and glenohumeral kinematics. *Journal of Electromyography and Kinesiology*, 16(3):224–235, 2006.

[28] David Eberly. Geometric tools engine. Source code, 2016.

[29] Kenji Emura, Takamitsu Arakawa, Akinori Miki, and Toshio Terashima. Anatomical observations of the human acromioclavicular joint. *Clinical Anatomy*, 27(7):1046–1052, 2014.

[30] Kenji Emura, Takamitsu Arakawa, Toshio Terashima, and Akinori Miki. Macroscopic and histological observations on the human sternoclavicular joint disc. *Anatomical Science International*, 84(3):182–188, 2009.

[31] A E Engin and S-M Chen. Statistical data base for the biomechanical properties of the human shoulder complexI: Kinematics of the shoulder complex. *Journal of Biomechanical Engineering*, 108:215–221, 1986.

[32] AE Engin and ST Tümer. Three-dimensional kinematic modelling of the human shoulder complexpart I: physical model and determination of joint sinus cones. *Journal of Biomechanical Engineering*, 111:107, 1989.

[33] Philippe Favre, Michael D Loeb, Naeder Helmy, and Christian Gerber. Latissimus dorsi transfer to restore external rotation with reverse shoulder arthroplasty: a biomechanical study. *Journal of Shoulder and Elbow Surgery*, 17(4):650–658, 2008.

[34] Fouad Fayad, Gilles Hoffmann, Sylvain Hanneton, Chadi Yazbeck, Marie-Martine Lefevre-colau, Serge Poiraudeau, Michel Revel, and Agnès Roby-Brami. 3-D scapular kinematics during arm elevation: effect of motion velocity. *Clinical Biomechanics*, 21(9):932–941, 2006.

[35] Jason R Fuller, Karen V Lomond, Joyce Fung, and Julie N Côté. Posture-movement changes following repetitive motion-induced shoulder muscle fatigue. *Journal of Electromyography and Kinesiology*, 19(6):1043–1052, 2009.

[36] Brian A Garner and Marcus G Pandy. A kinematic model of the upper limb based on the Visible Human Project (VHP) image dataset. *Computer Methods in Biomechanics and Biomedical Engineering*, 2(2):107–124, 1999.

[37] Brian A Garner and Marcus G Pandy. Musculoskeletal model of the upper limb based on the visible human male dataset. *Computer Methods in Biomechanics and Biomedical Engineering*, 4(2):93–126, 2001.

[38] Matthew A Gast and Sandra K Moore. A glimpse from the inside of a space suit: What is it really like to train for an EVA? *Acta Astronautica*, 68(1):316–325, 2011.

[39] Tej-Jaskirat Grewal and Clark R Dickerson. A novel three-dimensional shoulder rhythm definition that includes overhead and axially rotated humeral postures. *Journal of Biomechanics*, 46(3):608–611, 2013.

[40] R Happee and FCT Van der Helm. The control of shoulder muscles during goal directed movements, an inverse dynamic analysis. *Journal of Biomechanics*, 28(10):1179–1191, 1995.

[41] Dustin D Hardwick and Catherine E Lang. Scapula and humeral movement patterns and their relationship with pain: a preliminary investigation. *International Journal of Therapy and Rehabilitation*, 18(4):210, 2011.

[42] Alexandra Marie Hilbert. Human-spacesuit interaction: Understanding astronaut shoulder injury. Master's thesis, Massachusetts Institute of Technology, 2015.

[43] AM Hill, AMJ Bull, RJ Dallalana, AL Wallace, and GR Johnson. Glenohumeral motion: review of measurement techniques. *Knee Surgery, Sports Traumatology, Arthroscopy*, 15(9):1137–1143, 2007.

[44] Christian Högfors, Dan Karlsson, and Bo Peterson. Structure and internal consistency of a shoulder model. *Journal of Biomechanics*, 28(7):767–777, 1995.

[45] Christian Högfors, Bo Peterson, Göran Sigholm, and Peter Herberts. Biomechanical model of the human shoulder jointII. The shoulder rhythm. *Journal of Biomechanics*, 24(8):699–709, 1991.

[46] Christian Högfors, Göran Sigholm, and Peter Herberts. Biomechanical model of the human shoulderI. Elements. *Journal of Biomechanics*, 20(2):157–166, 1987.

[47] A Holtermann, PJ Mork, LL Andersen, Henrik Baare Olsen, and K Søgaard. The use of EMG biofeedback for learning of selective activation of intra-muscular parts within the serratus anterior muscle: a novel approach for rehabilitation of scapular muscle imbalance. *Journal of Electromyography and Kinesiology*, 20(2):359–365, 2010.

[48] Andreas Holtermann, Karin Roeleveld, Paul Jarle Mork, Christer Grönlund, J Stefan Karlsson, Lars L Andersen, Henrik Baare Olsen, Mette K Zebis, Gisela Sjøgaard, and Karen Søgaard. Selective activation of neuromuscular compartments within the human trapezius muscle. *Journal of Electromyography and Kinesiology*, 19(5):896–902, 2009.

[49] Katherine RS Holzbaur, Wendy M Murray, and Scott L Delp. A model of the upper extremity for simulating musculoskeletal surgery and analyzing neuromuscular control. *Annals of Biomedical Engineering*, 33(6):829–840, 2005.

[50] David Ingram, Christoph Engelhardt, Alain Farron, Alexandre Terrier, and Philippe Müllhaupt. A minimal set of coordinates for describing humanoid shoulder motion. In *Intelligent Robots and Systems (IROS), 2013 IEEE/RSJ International Conference on*, pages 5537–5544. IEEE, 2013.

[51] David Ingram, Christoph Engelhardt, Alain Farron, Alexandre Terrier, and Philippe Müllhaupt. Modelling of the human shoulder as a parallel mechanism without constraints. *Mechanism and Machine Theory*, 100:120–137, 2016.

[52] Verne T Inman, LeRoy C Abbott, et al. Observations on the function of the shoulder joint. *The Journal of Bone and Joint Surgery*, 26(1):1–30, 1944.

[53] J Jerosch, J Steinbeck, H Clahsen, M Schmitz-Nahrath, and A Grosse-Hackmann. Function of the glenohumeral ligaments in active stabilisation of the shoulder joint. *Knee Surgery, Sports Traumatology, Arthroscopy*, 1(3):152–158, 1993.

[54] Andrew R Karduna, Phil W McClure, Lori A Michener, and Brian Sennett. Dynamic measurements of three-dimensional scapular kinematics: a validation study. *Journal of Biomechanical Engineering*, 123(2):184–190, 2001.

[55] W. Ben Kibler, Paula M. Ludewig, Phil McClure, Tim L. Uhl, and Aaron Sciascia. Scapular summit 2009. *Journal of Orthopaedic & Sports Physical Therapy*, 39(11):A1–A13, 07 2009. PMID: 19881011.

[56] W Ben Kibler, Paula M Ludewig, Phil W McClure, Lori A Michener, Klaus Bak, Aaron D Sciascia, David Ebaugh, Jed Kuhn, et al. Clinical implications of scapular dyskinesis in shoulder injury: the 2013 consensus statement from the 'scapular summit'. *British Journal of Sports Medicine*, 47:877–885, 2013.

[57] Bongsu Kim and Ashish D Deshpande. Controls for the shoulder mechanism of an upper-body exoskeleton for promoting scapulohumeral rhythm. In *Rehabilitation Robotics (ICORR), 2015 IEEE International Conference on*, pages 538–542. IEEE, 2015.

[58] Bongsu Kim and Ashish D Deshpande. An upper-body rehabilitation exoskeleton Harmony with an anatomical shoulder mechanism: Design, modeling, control, and performance evaluation. *The International Journal of Robotics Research*, 36(4):414–435, 2017.

[59] Verena Klamroth-Marganska, Javier Blanco, Katrin Campen, Armin Curt, Volker Dietz, Thierry Ettlin, Morena Felder, Bernd Fellinghauer, Marco Guidali, Anja Kollmar, Andreas Luft, Tobias Nef, Corina Schuster-Amft, Werner Stahel, and Robert Riener. Three-dimensional, task-specific robot therapy of the arm after stroke: a multicentre, parallel-group randomised trial. *The Lancet Neurology*, 13(2):159–166, 2014.

[60] Mary D Klein Breteler, Cornelis W Spoor, and Frans CT Van der Helm. Measuring muscle and joint geometry parameters of a shoulder for modeling purposes. *Journal of biomechanics*, 32(11):1191–1197, 1999.

[61] Nives Klopčar and Jadran Lenarčič. Bilateral and unilateral shoulder girdle kinematics during humeral elevation. *Clinical Biomechanics*, 21:S20–S26, 2006.

[62] Nives Klopčar, Martin Tomšič, and Jadran Lenarčič. A kinematic model of the shoulder complex to evaluate the arm-reachable workspace. *Journal of Biomechanics*, 40(1):86–91, 2007.

[63] NA Langrana. Spatial kinematic analysis of the upper extremity using a biplanar videotaping method. *Journal of Biomechanical Engineering*, 103(1):11–17, 1981.

[64] Rebekah L. Lawrence, Jonathan P. Braman, Robert F. LaPrade, and Paula M. Ludewig. Comparison of 3-dimensional shoulder complex kinematics in individuals with and without shoulder pain, part 1: Sternoclavicular, acromioclavicular, and scapulothoracic joints. *Journal of Orthopaedic & Sports Physical Therapy*, 44(9):636–645, 2014.

[65] Rebekah L. Lawrence, Jonathan P. Braman, Justin L. Staker, Robert F. LaPrade, and Paula M. Ludewig. Comparison of 3-dimensional shoulder complex kinematics in individuals with and without shoulder pain, part 2: Glenohumeral joint. *Journal of Orthopaedic & Sports Physical Therapy*, 44(9):646–655, 2014.

[66] Mathieu Lempereur, Sylvain Brochard, Fabien Leboeuf, and Olivier Rémy-Néris. Validity and reliability of 3D marker based scapular motion analysis: a systematic review. *Journal of Biomechanics*, 47(10):2219–2230, 2014.

[67] Jadran Lenarčič and Michael Stanišić. A humanoid shoulder complex and the humeral pointing kinematics. *IEEE Transactions on Robotics and Automation*, 19(3):499–506, 2003.

[68] Ho Shing Lo and Sheng Quan Xie. Exoskeleton robots for upper-limb rehabilitation: State of the art and future prospects. *Medical Engineering & Physics*, 34(3):261–268, 2012.

[69] T-W Lu and JJ OConnor. Bone position estimation from skin marker coordinates using global optimisation with joint constraints. *Journal of Biomechanics*, 32(2):129–134, 1999.

[70] Paula M Ludewig, Vandana Phadke, Jonathan P Braman, Daniel R Hassett, Cort J Cieminski, and Robert F LaPrade. Motion of the shoulder complex during multiplanar humeral elevation. *The Journal of Bone & Joint Surgery*, 91(2):378–389, 2009.

[71] Amy Cole Lukasiewicz, Philip McClure, Lori Michener, Neal Pratt, and Brian Sennett. Comparison of 3-dimensional scapular position and orientation between subjects with and without shoulder impingement. *Journal of Orthopaedic & Sports Physical Therapy*, 29(10):574–586, 1999.

[72] Peter Lum, David Reinkensmeyer, Richard Mahoney, William Z. Rymer, and Charles Burgar. Robotic devices for movement therapy after stroke: current status and challenges to clinical acceptance. *Topics in Stroke Rehabilitation*, 8(4):40–53, 2002.

[73] Paweł Maciejasz, Jörg Eschweiler, Kurt Gerlach-Hahn, Arne Jansen-Troy, and Steffen Leonhardt. A survey on robotic devices for upper limb rehabilitation. *Journal of NeuroEngineering and Rehabilitation*, 11(1), 2014.

[74] Sandro Scattareggia Marchese. *Sterno-clavicular kinematics: a new measurement system.* PhD thesis, University of Newcastle upon Tyne, 2000.

[75] Daniel F Massimini, Jon JP Warner, and Guoan Li. Non-invasive determination of coupled motion of the scapula and humerusan in-vitro validation. *Journal of Biomechanics*, 44(3):408–412, 2011.

[76] Ricardo Matias, Carlos Andrade, and António Prieto Veloso. A transformation method to estimate muscle attachments based on three bony landmarks. *Journal of Biomechanics*, 42(3):331–335, 2009.

[77] Ricardo Matias and Augusto Gil Pascoal. The unstable shoulder in arm elevation: a three-dimensional and electromyographic study in subjects with glenohumeral instability. *Clinical Biomechanics*, 21:S52–S58, 2006.

[78] Walter Maurel and Daniel Thalmann. Human shoulder modeling including scapulo-thoracic constraint and joint sinus cones. *Computers & Graphics*, 24(2):203–218, 2000.

[79] Philip W McClure, Lori A Michener, Brian J Sennett, and Andrew R Karduna. Direct 3-dimensional measurement of scapular kinematics during dynamic movements in vivo. *Journal of Shoulder and Elbow Surgery*, 10(3):269–277, 2001.

[80] Jennifer L McGinley, Richard Baker, Rory Wolfe, and Meg E Morris. The reliability of three-dimensional kinematic gait measurements: a systematic review. *Gait & Posture*, 29(3):360–369, 2009.

[81] Kevin J McQuade, John Borstad, and Anamaria Siriani de Oliveira. Critical and theoretical perspective on scapular stabilization: What does it really mean, and are we on the right track? *Physical Therapy*, 96(8):1162, 2016.

[82] Kevin J McQuade, Jeffrey Dawson, and Gary L Smidt. Scapulothoracic muscle fatigue associated with alterations in scapulohumeral rhythm kinematics during maximum resistive shoulder elevation. *Journal of Orthopaedic & Sports Physical Therapy*, 28(2):74–80, 1998.

[83] Kevin J McQuade and Gary L Smidt. Dynamic scapulohumeral rhythm: the effects of external resistance during elevation of the arm in the scapular plane. *Journal of Orthopaedic & Sports Physical Therapy*, 27(2):125–133, 1998.

[84] Jan Mehrholz, Anja Hädrich, Thomas Platz, Joachim Kugler, and Marcus Pohl. Electromechanical and robot-assisted arm training for improving generic activities of daily living, arm function, and arm muscle strength after stroke. *The Cochrane Library*, 2012.

[85] CGM Meskers, HM Vermeulen, JH De Groot, FCT Van der Helm, and PM Rozing. 3D shoulder position measurements using a six-degree-of-freedom electromagnetic tracking device. *Clinical Biomechanics*, 13(4-5):280–292, 1998.

[86] Lori A Michener, Philip W McClure, and Andrew R Karduna. Anatomical and biomechanical mechanisms of subacromial impingement syndrome. *Clinical Biomechanics*, 18(5):369–379, 2003.

[87] Thomas B Moeslund, Claus B Madsen, and Erik Granum. Modelling the 3D pose of a human arm and the shoulder complex utilising only two parameters. *Integrated Computer-Aided Engineering*, 12(2):159–175, 2005.

[88] Siegfried Mollier. *Über die Statik und Mechanik des menschlichen Schultergürtels unter normalen und pathologischen Verhältnissen: Mit 7 Tabellen.* Fischer, 1899.

[89] Joseph B Myers, Craig A Wassinger, and Scott M Lephart. Sensorimotor contribution to shoulder stability: effect of injury and rehabilitation. *Manual Therapy*, 11(3):197–201, 2006.

[90] Tobias Nef, Marco Guidali, and Robert Riener. ARMin III–arm therapy exoskeleton with an ergonomic shoulder actuation. *Applied Bionics and Biomechanics*, 6(2):127–142, 2009.

[91] Jeremy T Newkirk and Michael M Stanišić. Design of a humanoid shoulder complex emulating human shoulder girdle motion using the minimum number of actuators. *International Journal of Humanoid Robotics*, 13(04):1550045, 2016.

[92] Ali Asadi Nikooyan, Frans CT van der Helm, Peter Westerhoff, Friedmar Graichen, Georg Bergmann, and HEJ Dirkjan Veeger. Comparison of two methods for in vivo estimation of the glenohumeral joint rotation center (GH-JRC) of the patients with shoulder hemiarthroplasty. *PLoS One*, 6(3), 2011.

[93] Matteo Paci, Luca Nannetti, and Lucio A Rinaldi. Glenohumeral subluxation in hemiplegia: An overview. *Journal of Rehabilitation Research and Development*, 42(4):557, 2005.

[94] Russ Paine and Michael L Voight. Invited clinical commentary. The role of the scapula. *International Journal of Sports Physical Therapy*, 8(5):617–629, 2013.

[95] Jacquelin Perry. Anatomy and biomechanics of the shoulder in throwing, swimming, gymnastics, and tennis. *Clinics in Sports Medicine*, 2(2):247–270, 1983.

[96] Dean M Plafcan, Patricia J Turczany, Blaine A Guenin, Sam Kegerreis, and Teddy W Worrell. An objective measurement technique for posterior scapular displacement. *Journal of Orthopaedic & Sports Physical Therapy*, 25(5):336–341, 1997.

[97] Gijs M Pronk. A kinematic model of the shoulder girdle: a resume. *Journal of Medical Engineering & Technology*, 13(1-2):119–123, 1989.

[98] GM Pronk and FCT Van der Helm. The palpator: an instrument for measuring the positions of bones in three dimensions. *Journal of Medical Engineering & Technology*, 15(1):15–20, 1991.

[99] Jeffery W Rankin, W Mark Richter, and Richard R Neptune. Individual muscle contributions to push and recovery subtasks during wheelchair propulsion. *Journal of Biomechanics*, 44(7):1246–1252, 2011.

[100] Yupeng Ren, Hyung-Soon Park, and Li-Qun Zhang. Developing a whole-arm exoskeleton robot with hand opening and closing mechanism for upper limb stroke rehabilitation. In *Rehabilitation Robotics (ICORR), 2009 IEEE International Conference on*, pages 761–765, 2009.

[101] Robert C Rhoad, John J Klimkiewicz, Gerald R Williams, Susan B Kesmodel, Jayaram K Udupa, J Bruce Kneeland, and Joseph P Iannotti. A new in vivo technique for three-dimensional shoulder kinematics analysis. *Skeletal Radiology*, 27(2):92–97, 1998.

[102] R Tyler Richardson, Elizabeth A Rapp, R Garry Quinton, Kristen F Nicholson, Brian A Knarr, Stephanie A Russo, Jill S Higginson, and James G Richards.

Errors associated with utilizing prescribed scapular kinematics to estimate unconstrained, natural upper extremity motion in musculoskeletal modeling. *Journal of Applied Biomechanics*, In press:1–18, 2017.

[103] A. Roby-Brami, A. Feydy, M. Combeaud, E. V. Biryukova, B. Bussel, and M. F. Levin. Motor compensation and recovery for reaching in stroke patients. *Acta Neurologica Scandinavica*, 107(5):369–381, 2003.

[104] Amy Ross. Z-1 prototype space suit testing summary. In *43rd International Conference on Environmental Systems*, pages 1–12, 2013.

[105] Peter J. Rundquist, Michelle Dumit, Jeannie Hartley, Kendall Schultz, and Margaret A. Finley. Three-dimensional shoulder complex kinematics in individuals with upper extremity impairment from chronic stroke. *Disability and Rehabilitation*, 34(5):402–407, 2012.

[106] Katherine R Saul, Xiao Hu, Craig M Goehler, Meghan E Vidt, Melissa Daly, Anca Velisar, and Wendy M Murray. Benchmarking of dynamic simulation predictions in two software platforms using an upper limb musculoskeletal model. *Computer Methods in Biomechanics and Biomedical Engineering*, 18(13):1445–1458, 2015.

[107] Rick Scheuring, Pat McCulloch, Mary Van Baalen, Richard Watson, Steve Bowen, and Terri Blatt. Shoulder injuries in US astronauts related to EVA suit design. In *83rd Annual Aerospace Medical Association Meeting*, 05 2012.

[108] Miroslav Šenk and Laurence Chèze. A new method for motion capture of the scapula using an optoelectronic tracking device: a feasibility study. *Computer Methods in Biomechanics and Biomedical Engineering*, 13(3):397–401, 2010.

[109] Ajay Seth, Ricardo Matias, António P Veloso, and Scott L Delp. A biomechanical model of the scapulothoracic joint to accurately capture scapular kinematics during shoulder movements. *PLoS One*, 11(1):e0141028, 2016.

[110] Victor Sholukha and Serge Van Sint Jan. Combined motions of the shoulder joint complex for model-based simulation: Modeling of the shoulder rhythm (ShRm). In *3D Multiscale Physiological Human*, pages 205–232. Springer, 2014.

[111] M Skreiner. Methods to identify the mobility regions of a spatial four-link mechanism. *Journal of Mechanisms*, 2(4):415–427, 1967.

[112] FCO Sticher. Mobility limit analysis of RSSR mechanisms by "ellipse diagram". *Journal of Mechanisms*, 5(3):393IN1415–414IN2, 1970.

[113] Haijun Su, CL Collins, and JM McCarthy. Classification of RRSS linkages. *Mechanism and Machine Theory*, 37(11):1413–1433, 2002.

[114] Bertrand Tondu. Modelling of the shoulder complex and application the design of upper extremities for humanoid robots. In *Humanoid Robots, 2005 5th IEEE-RAS International Conference on*, pages 313–320. IEEE, 2005.

[115] Andras Toth, Gabor Fazekas, Gusztav Arz, Mihaly Jurak, and Monika Horvath. Passive robotic movement therapy of the spastic hemiparetic arm with REHAROB: report of the first clinical test and the follow-up system improvement. In *Rehabilitation Robotics (ICORR), 2005 IEEE International Conference on*, pages 127–130, 2005.

[116] ST Tümer and AE Engin. Three-dimensional kinematic modeling of the human shoulder complex-part II: Mathematical modelling and solution via optimization. *Journal of Biomechanical Engineering*, 111:113–121, 1989.

[117] Frans CT van der Helm. A finite element musculoskeletal model of the shoulder mechanism. *Journal of Biomechanics*, 27(5):551–569, 1994.

[118] Jon JP Warner, Lyle J Micheli, Linda E Arslanian, John Kennedy, and Richard Kennedy. Scapulothoracic motion in normal shoulders and shoulders with glenohumeral instability and impingement syndrome a study using Moiré topographic analysis. *Clinical Orthopaedics and Related Research*, 285:191–199, 1992.

[119] David R Williams and Brian J Johnson. EMU shoulder injury tiger team report. Technical Report NASA/TM-2003-212058, S-912, NASA Johnson Space Center, 09 2003.

[120] RL Williams and CF Reinholtz. Mechanism link rotatability and limit position analysis using polynomial discriminants. *Journal of Mechanisms, Transmissions, and Automation in design*, 109(2):178–182, 1987.

[121] JE Wood, Sanford G Meek, and SC Jacobsen. Quantitation of human shoulder anatomy for prosthetic arm controlI. surface modelling. *Journal of Biomechanics*, 22(3):273–292, 1989.

[122] Ge Wu, Frans CT Van der Helm, HEJ DirkJan Veeger, Mohsen Makhsous, Peter Van Roy, Carolyn Anglin, Jochem Nagels, Andrew R Karduna, Kevin McQuade, Xuguang Wang, Frederick W Werner, and Bryan Buchholz. ISB

recommendation on definitions of joint coordinate systems of various joints for the reporting of human joint motion–Part II: shoulder, elbow, wrist and hand. *Journal of Biomechanics*, 38(5):981–992, 2005.

[123] Xu Xu, Clark R Dickerson, Jia-hua Lin, and Raymond W McGorry. Evaluation of regression-based 3-D shoulder rhythms. *Journal of Electromyography and Kinesiology*, 29:28–33, 2016.

[124] Xu Xu, Jia-hua Lin, and Raymond W McGorry. A regression-based 3-D shoulder rhythm. *Journal of Biomechanics*, 47(5):1206–1210, 2014.

[125] Lu Yang. Recent advances on determining the number of real roots of parametric polynomials. *Journal of Symbolic Computation*, 28(1-2):225–242, 1999.

[126] James W Youdas, James R Carey, Tom R Garrett, and Vera J Suman. Reliability of goniometric measurements of active arm elevation in the scapular plane obtained in a clinical setting. *Archives of Physical Medicine and Rehabilitation*, 75(10):1137–1144, 1994.

Vita

Evan Michael Ogden was born in Cincinnati, Ohio and grew up in San Antonio, Texas. He attended The University of Texas at Austin for his undergraduate studies and earned a Bachelor of Science in Mechanical Engineering with Highest Honors in May 2014. In August 2014, he entered the Mechanical Engineering Graduate Program at The University of Texas at Austin. He is a NASA Space Technology Research Fellow for research on shoulder modeling and control methods for robotic exoskeletons.

Email address: emogden@utexas.edu

This thesis was typeset with LaTeXby the author.